Available online at www.sciencedirect.com

ScienceDirect

Nuclear Physics B 943 (2019) 114612

NUCLEAR PHYSICS B

www.elsevier.com/locate/nuclphysb

How perturbative are heavy sea quarks?

ALPHA Collaboration

Andreas Athenodorou [a,b], Jacob Finkenrath [b], Francesco Knechtli [c,*], Tomasz Korzec [c], Björn Leder [d], Marina Krstić Marinković [e], Rainer Sommer [f,d]

[a] *Department of Physics, University of Cyprus, P.O. Box 20537, Nicosia CY, Cyprus*
[b] *CaSToRC, CyI Athalassa Campus, 20 Constantinou Kavafi Street, 2121 Nicosia, Cyprus*
[c] *Department of Physics, Bergische Universität Wuppertal, Gaussstr. 20, 42119 Wuppertal, Germany*
[d] *Institut für Physik, Humboldt-Universität zu Berlin, Newtonstr. 15, 12489 Berlin, Germany*
[e] *School of Mathematics, Trinity College, Dublin 2, Ireland*
[f] *John von Neumann Institute for Computing (NIC), DESY, Platanenallee 6, D-15738 Zeuthen, Germany*

Received 19 September 2018; received in revised form 25 March 2019; accepted 7 April 2019
Available online 10 April 2019
Editor: Tommy Ohlsson

Abstract

Effects of heavy sea quarks on the low energy physics are described by an effective theory where the expansion parameter is the inverse quark mass, $1/M$. At leading order in $1/M$ (and neglecting light quark masses) the dependence of any low energy quantity on the heavy quark mass is given in terms of the ratio of Λ parameters of the effective and the fundamental theory. We define a function describing the scaling with the mass M. Our study of perturbation theory suggests that its perturbative expansion is very reliable for the bottom quark and also seems to work very well at the charm quark mass. The same is then true for the ratios of $\Lambda^{(4)}/\Lambda^{(5)}$ and $\Lambda^{(3)}/\Lambda^{(4)}$, which play a major rôle in connecting (almost all) lattice determinations of $\alpha^{(3)}_{\overline{\rm MS}}$ from the three-flavor theory with $\alpha^{(5)}_{\overline{\rm MS}}(M_{\rm Z})$. Also the charm quark content of the nucleon, relevant for dark matter searches, can be computed accurately from perturbation theory.

In order to further test perturbation theory in this situation, we investigate a very closely related model, namely QCD with $N_{\rm f} = 2$ heavy quarks. Our non-perturbative information is derived from simulations on the lattice, with masses up to the charm quark mass and lattice spacings down to about 0.023 fm followed by a continuum extrapolation. The non-perturbative mass dependence agrees within rather small errors

* Corresponding author.
E-mail address: knechtli@physik.uni-wuppertal.de (F. Knechtli).

https://doi.org/10.1016/j.nuclphysb.2019.114612

with the perturbative prediction at masses around the charm quark mass. Surprisingly, from studying solely the massive theory we can make a prediction for the ratio $Q_{0,2}^{1/\sqrt{t_0}} = [\Lambda\sqrt{t_0(0)}]_{N_f=2}/[\Lambda\sqrt{t_0}]_{N_f=0}$, which refers to the chiral limit in $N_f = 2$. Here t_0 is the Gradient Flow scale of [1]. The uncertainty for Q is estimated to be 2.5%. For the phenomenologically interesting $\Lambda^{(3)}/\Lambda^{(4)}$, we conclude that perturbation theory introduces errors which are at most at the 1.5% level, smaller than other current uncertainties.

1. Introduction

At present most simulations of lattice Quantum Chromodynamics (QCD) include two light (up and down) quarks and a strange quark. It is important to investigate the effects of the charm quark, whose mass M is about 12 times larger than that of the strange quark. Effective field theory [2] arguments predict that the effects of a heavy quark are described by the theory without the heavy quark with leading order power corrections of size $O(1/M^2)$. At lowest order in $1/M$ only the light quark masses and the coupling need to be adjusted to match the two theories (with and without the heavy quarks). For the coupling this issue has been discussed in perturbation theory in [3]. The matching of the coupling in the case of the decoupling of one heavy quark is known to four loops in perturbation theory [4,5]. Equivalently to match the couplings at a given renormalization scale one can formulate a relation between the renormalization group invariant Λ parameters of the effective and the fundamental theory. In this article we present a study of the perturbative behavior of the ratio of Λ parameters computed up to four loops in the matching of the couplings, which requires the knowledge of the five loop β function, which had been computed in Refs. [6–10].

Besides studying the behavior of perturbation theory itself it is desirable to compare to non-perturbative data. This is especially the case for the charm quark given that matching is performed at a fairly low scale $\approx 1.3\,\text{GeV}$ in this case. It is very difficult to compare directly 2+1 flavor and 2+1+1 flavor lattice simulations, because various systematic uncertainties mask the physical effect. We proposed instead to simulate a model, namely QCD with two heavy, mass-degenerate quarks [11]. The effective theory is the Yang-Mills theory up to $1/M^2$ corrections. The mass dependence of ratios of hadronic scales such as $\sqrt{t_0(0)}/\sqrt{t_0(M)}$, where t_0 is the Gradient flow scale [1] factorizes [11] at leading order in a non-perturbative and mass-independent factor, and a factor P, which is the ratio of the Λ parameters and depends on the heavy quark mass through the matching. Since the latter can be evaluated in perturbation theory we can compare the perturbative mass dependence of hadronic scales to the non-perturbative results from the simulations. We define a mass-scaling function which is the logarithmic derivative of P with respect to the logarithm of the mass. It can be determined directly from the simulations and compared to its perturbative expansion.

This article is organized as follows. In section 2 we describe the effective theory of decoupling. Section 3 contains a review of the matching of the effective and fundamental theory at leading order. We present a perturbative study of the ratio P of the Λ parameters, which results from the matching of the theories at leading order, and of the mass-scaling function. In section 4 we explain our non-perturbative study of decoupling in a theory with $N_f = 2$ mass-degenerate heavy fermions with masses ranging up to (slightly above) the charm quark mass. We introduce the hadronic scales which we calculate in Monte Carlo simulations of lattice QCD and give details of the lattice simulations. The comparison of the non-perturbative mass dependence of

hadronic scales computed from the simulations with perturbation theory is presented in section 5. The implications of these results for the applicability of perturbation theory at the scale of the charm quark mass are discussed in section 6. We summarize our results in section 7. In the appendix A we reproduce the explicit formulae for the matching of the couplings up to four loops and the perturbative coefficients of the mass-scaling function. The asymptotic behavior for large masses of P is derived in appendix B. Finally appendix C contains tables listing the simulations parameters.

2. The effective theory: decQCD

The effective theory associated with the decoupling of heavy quarks is formally obtained by integrating out the heavy quark fields. The resulting effective theory contains a tower of non-renormalizable interactions, which however are suppressed at low energies by negative powers of the heavy quark masses [2]. The (infinite number of) couplings of the effective theory can be matched order by order and used to describe the effect of heavy quarks at low energies.

To be precise, let us consider $\mathrm{QCD}_{N_\mathrm{f}}$ with N_f quarks in total, of which N_ℓ are light and $N_\mathrm{f}-N_\ell$ are heavy. For simplicity we assume the light and the heavy quarks to be mass degenerate with the heavy mass given by M. Non-degenerate quark masses are conceptually similar, see note at the end of this section. In general the Lagrangian of the effective theory is

$$\mathcal{L}_\mathrm{dec} = \mathcal{L}_0 + \frac{1}{M}\mathcal{L}_1 + \frac{1}{M^2}\mathcal{L}_2 + \dots , \tag{2.1}$$

where the leading order equals QCD_{N_ℓ} with N_ℓ quarks and the corrections $\mathcal{L}_k$, $k \geq 1$ consist of linear combinations of local operators of dimension $4+k$. These operators are composed of only the light quark and gauge fields, and include possible light mass factors. They have to satisfy the symmetries of $\mathrm{QCD}_{N_\mathrm{f}}$, most prominently gauge, Euclidean (or Lorentz) and chiral invariance. For the cases of interest, operators of dimension five are excluded and corrections to the leading order start at $\mathrm{O}(M^{-2})$

$$\mathcal{L}_\mathrm{dec} = \mathcal{L}_{\mathrm{QCD}_{N_\ell}} + \frac{1}{M^2}\sum_i \omega_i \Phi_i + \dots . \tag{2.2}$$

Here we write $\mathcal{L}_2$ explicitly as a linear combination of local dimension six operators Φ_i, multiplied by dimensionless couplings ω_i.

The simplest situation in which (2.2) holds is $N_\ell = 0$, i.e., when light quarks are absent: the leading order is Yang-Mills theory and there is no gauge invariant dimension five operator made up of gauge fields alone. Thus at leading order only the gauge coupling has to be matched. We are basing our non-perturbative investigations in sections 4-5 on this setting.

In the presence of $N_\ell \geq 2$ mass-less quarks the non-singlet, non-anomalous chiral symmetry in the light quark sector forbids any dimension five operator. The gauge coupling is still the only coupling to be matched at leading order. Note that the dynamical (non-perturbative) breaking of chiral symmetry plays no role here as we may consider full and effective theory in a finite (but large) volume where dynamical symmetry breaking is absent, in full analogy with the elegant derivation of automatic $\mathrm{O}(a)$ improvement of twisted mass QCD in [12]. More explicitly consider a chirally non-invariant observable in the full theory in finite volume. It vanishes, while a priori in the effective theory at dimension five the Pauli term $\omega_\mathrm{Pauli}\bar{\psi} i\sigma_{\mu\nu}F_{\mu\nu}\psi/M$ contributes as the only dimension five gauge invariant operator. Matching of full and effective theory requires $\omega_\mathrm{Pauli} = 0$.

In section 3 we consider the leading order in $1/M$ in perturbation theory for various values of N_ℓ, $N_{\rm f}$.

For finite light quark masses there are dimension five operators, which are formed of the operators in $\mathcal{L}_{{\rm QCD}_{N_\ell}}$ multiplied by the light quark masses. Their effect can be absorbed in a redefinition of the gauge coupling and light quark masses at the order $m_{\rm l}/M$. The Pauli term multiplied by the light quark masses contributes at dimension six. It is one of the Φ_i in eq. (2.2). Besides the gauge coupling now also the light quark mass needs to be matched.

All in all, finite light quark masses do not change the structure of eq. (2.2). Of course couplings in the effective Lagrangian now also depend on the light quark mass. The only restriction is that when light quarks are present, we need at least a doublet, such that there is a non-anomalous chiral symmetry of the mass-less theory and we can conclude $\omega_{\rm Pauli} = 0$ as sketched above.

In the following we concentrate on $N_\ell \geq 2$ mass-less or $N_\ell = 0$ quarks.

3. Mass-dependence in the leading order effective theory

At leading order, the only parameter of the effective theory, ${\rm QCD}_{N_\ell}$, is its running coupling and the theory predicts all observables when the coupling is prescribed at a given renormalization scale in a given renormalization scheme. It is conceptually cleaner, but completely equivalent in terms of the physical content to specify the renormalization group invariant (RGI) Λ-parameter. The scale dependence of the input is then gone and the scheme-dependence is easily computable: the one-loop relation of couplings yields the exact relation of the associated Λ-parameters.

Explicitly the Λ-parameter of QCD with $N_{\rm f}$ quarks,

$$\Lambda_{\rm f} = \mu \left(b_0 \bar{g}^2\right)^{-b_1/(2b_0^2)} {\rm e}^{-1/(2b_0\bar{g}^2)} \exp\left\{ -\int_0^{\bar{g}} {\rm d}x \left[\frac{1}{\beta_{\rm f}(x)} + \frac{1}{b_0 x^3} - \frac{b_1}{b_0^2 x} \right] \right\} , \tag{3.1}$$

is defined as the integration constant of the solution to the renormalization group equation (RGE)

$$\mu \frac{\partial \bar{g}}{\partial \mu} = \beta_{\rm f}(\bar{g}) \tag{3.2}$$

for the renormalized coupling $\bar{g}$ at renormalization scale μ with the QCD β-function

$$\beta_{\rm f}(\bar{g}) \overset{\bar{g}\to 0}{\sim} -\bar{g}^3 \left\{ b_0 + \bar{g}^2 b_1 + \ldots \right\} , \tag{3.3}$$

$$b_0 = \frac{1}{(4\pi)^2}\left(11 - \frac{2}{3}N_{\rm f}\right) , \quad b_1 = \frac{1}{(4\pi)^4}\left(102 - \frac{38}{3}N_{\rm f}\right) .$$

We shall also make use of the RGI mass

$$M = \overline{m}\,(2b_0\bar{g}^2)^{-d_0/(2b_0)} \exp\left\{ -\int_0^{\bar{g}} {\rm d}x \left[\frac{\tau_{\rm f}(x)}{\beta_{\rm f}(x)} - \frac{d_0}{b_0 x} \right] \right\} \tag{3.4}$$

which appears as an integration constant in the solution of the RGE

$$\frac{\mu}{\overline{m}} \frac{\partial \overline{m}}{\partial \mu} = \tau_{\rm f}(\bar{g}) , \tag{3.5}$$

$$\tau_{\rm f}(\bar{g}) \overset{\bar{g}\to 0}{\sim} -\bar{g}^2 \left\{ d_0 + \bar{g}^2 d_1 + \ldots \right\} , \qquad d_0 = 8/(4\pi)^2 , \tag{3.6}$$

for the renormalized mass at scale μ. Amongst different mass definitions, the RGI mass is distinguished by scale and scheme independence and represents our choice to discuss mass-dependences. The above holds in any mass-independent renormalization scheme.

In the following subsection we discuss how the relation of the Λ-parameters of fundamental and effective theory determine the (heavy-) mass dependence of low energy observables and then turn to the available perturbative information. This serves to prepare for our subsequent non-perturbative investigation.

3.1. Non-perturbative matching and mass-dependence

The leading order (in $1/M$) effective theory describes the fundamental one at low energy when Λ_ℓ has the proper value. In other words, it has to be chosen as a function of M and $\Lambda_{\rm f}$. To make that precise, we specify the Λ-parameters in units of an arbitrary (but low energy) mass scale $\mathcal{S}$. One may think of a hadron mass or low energy scales such as r_0^{-1}, $t_0^{-1/2}$, w_0^{-1} [1,13,14]. The relation between the Λ-parameters of fundamental and effective theory may then be written as

$$\frac{\Lambda_\ell}{\mathcal{S}_\ell} = P^{\mathcal{S}}_{\ell,{\rm f}}(M/\Lambda_{\rm f}) \times \frac{\Lambda_{\rm f}}{\mathcal{S}_{\rm f}(M)}\,. \tag{3.7}$$

Since ratios of low energy scales are the same in the leading order effective theory and in the fundamental theory,[1]

$$\frac{\mathcal{S}_{\rm f}(M)}{\mathcal{S}'_{\rm f}(M)} = \frac{\mathcal{S}_\ell}{\mathcal{S}'_\ell} + {\rm O}((\Lambda_{\rm f}/M)^2)\,, \tag{3.8}$$

we may also omit the units and write

$$\Lambda_\ell = P_{\ell,{\rm f}}(M/\Lambda_{\rm f})\,\Lambda_{\rm f}\,, \tag{3.9}$$

remembering that (non-perturbatively) $P_{\ell,{\rm f}}(M/\Lambda_{\rm f})$ has an ${\rm O}((\Lambda_{\rm f}/M)^2)$ fuzziness and that the Λ's have to be measured in units of the same low energy scale in the two theories. One may also read eq. (3.9) in this way: once the intrinsic non-perturbative scale of the fundamental theory is specified the equation determines the one of the effective theory through the factor $P_{\ell,{\rm f}}(M/\Lambda_{\rm f})$. Note that by definition the Λ-parameter of the fundamental theory does not depend on M, but the value of the dimensionful Λ-parameter in the effective theory Λ_ℓ does depend on it through eq. (3.9).

Multiplication of eq. (3.7) with $\mathcal{S}_{\rm f}(0)/\Lambda_{\rm f}$ yields the interesting equation

$$\begin{aligned}\frac{\mathcal{S}_{\rm f}(M)}{\mathcal{S}_{\rm f}(0)} &= Q^{\mathcal{S}}_{\ell,{\rm f}} \times P^{\mathcal{S}}_{\ell,{\rm f}}(M/\Lambda_{\rm f}) \\ &= Q^{\mathcal{S}}_{\ell,{\rm f}} \times P_{\ell,{\rm f}}(M/\Lambda_{\rm f}) + {\rm O}((\Lambda_{\rm f}/M)^2)\,.\end{aligned} \tag{3.10}$$

with

$$Q^{\mathcal{S}}_{\ell,{\rm f}} = \frac{\mathcal{S}_\ell/\Lambda_\ell}{\mathcal{S}_{\rm f}(0)/\Lambda_{\rm f}} \tag{3.11}$$

defined entirely through the two mass-less theories. The ratio $\frac{\mathcal{S}_{\rm f}(M)}{\mathcal{S}_{\rm f}(0)}$ can be computed in the fundamental theory and eq. (3.10) is a consequence of decoupling which can be tested. We call

[1] Such ratios are independent of the value of the coupling constant.

eq. (3.10) *factorization formula* because it separates the mass dependence into a "perturbative" (see section 3.2) factor $P_{\ell,\mathrm{f}}$ and a non-perturbative factor $Q^{\mathcal{S}}_{\ell,\mathrm{f}}$ respectively. In the same loose sense as usually used in factorization formulae, the long-distance physics is in Q while the short-distance one is in P. The scale for long/short is given by $1/M$. We have "perturbative" in quotes, because the meaning is not that perturbation theory gives the complete answer but that it yields an asymptotic expansion.

To simplify the notation, we will from now on omit the subscripts ℓ, f when referring to the quantities Q, P.

In phenomenology, eq. (3.10) does not seem interesting since one is usually not interested in the, e.g., proton mass at vanishing charm- or bottom-quark mass. However, in non-perturbative studies of QCD for different flavors the ratio Q is a natural quantity to determine, and is known to some degree, see below. Testing eq. (3.10) is thus a natural question. Furthermore, taking a logarithmic derivative of the nucleon mass w.r.t. the mass M yields the charm content in the nucleon, see Sect. 6.3.

Indeed we will study the mass-scaling function ($P'(x) = \frac{\mathrm{d}}{\mathrm{d}x} P(x)$)

$$\eta^{\mathrm{M}}(M) \equiv \frac{M}{P} \left.\frac{\partial P}{\partial M}\right|_{\Lambda_{\mathrm{f}}} = \frac{M}{\Lambda_{\mathrm{f}}} \frac{P'}{P}\,, \tag{3.12}$$

which can be computed in perturbation theory when M is sufficiently large, cf. [15].

We can estimate η^{M} from the mass dependence of hadronic quantities by taking the logarithmic derivative in eq. (3.10) with respect to the mass

$$\left.\frac{M}{\mathcal{S}_{\mathrm{f}}} \frac{\partial \mathcal{S}_{\mathrm{f}}}{\partial M}\right|_{\Lambda_{\mathrm{f}}} = \eta^{\mathrm{M}}\,, \tag{3.13}$$

where $\mathcal{S}_{\mathrm{f}}(0)$ and Q drop out. Their uncertainties play no role and we will therefore be able to make a more stringent comparison between perturbation theory and the full theory. Of course the Λ^2/M^2 dependence of $\mathcal{S}$ in eq. (3.10) is inherited by η^{M}.

3.2. Perturbation theory

We consider a mass-independent renormalization scheme; whenever we insert perturbative coefficients, it will be in the $\overline{\mathrm{MS}}$-scheme. To simplify notation we use $\bar{g}(\mu/\Lambda) \equiv \overline{g}_{\mathrm{f}}(\mu/\Lambda_{\mathrm{f}})$.

3.2.1. Matching of couplings

In general form, the relation between the couplings $\bar{g}(\mu/\Lambda)$ of the fundamental theory and $\overline{g}_\ell(\mu/\Lambda_\ell)$ of the leading order effective theory reads

$$\overline{g}^2_\ell(\mu/\Lambda_\ell) = F(\bar{g}^2(\mu/\Lambda), M/\Lambda)\,. \tag{3.14}$$

In principle the function F depends on which low energy observable is matched as discussed in the previous section for $P^{\mathcal{S}}_{\ell,\mathrm{f}}$. However, that dependence is only through powers of μ_{match}/M, where μ_{match} is the typical energy scale of the matched observable. In perturbation theory $(\mu_{\mathrm{match}}/M)^n$ terms can uniquely be separated from the logarithmic $\bar{g}^2$ terms. Dropping the power corrections as appropriate for the leading order theory, the coupling relation (i.e. the function F) is thus universal, i.e. independent of the matching condition.

Choosing the particular scale $\mu = m_*$ [2,3] in eq. (3.14), the first order perturbative correction vanishes in the $\overline{\mathrm{MS}}$ scheme and we have [4,16]

$$\overline{g}_\ell^2(m_*/\Lambda_\ell) = g_*^2\, C(g_*)\,, \quad g_* \equiv \bar{g}(m_*/\Lambda)\,, \tag{3.15}$$

$$C(x) = 1 + c_2 x^4 + c_3 x^6 + c_4 x^8 + \dots \quad . \tag{3.16}$$

The scale m_* is defined such that the running $\bar{\text{MS}}$ quark mass fulfills $\overline{m}(m_*) = m_*$. The two loop coefficient is then given by $c_2 = (N_\text{f} - N_\ell)\,\frac{11}{72}\,(4\pi^2)^{-2}$. The coefficients c_3 and c_4 are known for $N_\text{f} - N_\ell = 1, 2$ and $N_\text{f} - N_\ell = 1$, respectively. They are listed in Appendix A. One should remember that through eq. (3.4), m_* and M are in one-to-one relation.

3.2.2. Mass scaling function η^M

In order to find the perturbative expansion of η^M, eq. (3.12), we start from the related function (considering $P(M/\Lambda) = P(M(m_*, \Lambda)/\Lambda)$)

$$\eta^\text{m} = \frac{m_*}{P}\,\frac{\partial P}{\partial m_*}\bigg|_\Lambda\,, \tag{3.17}$$

which appears upon taking a derivative with respect to the logarithm of m_* on both sides of eq. (3.15). The left hand side yields

$$m_*\frac{\partial \overline{g}_\ell^2}{\partial m_*} = 2\overline{g}_\ell \beta_\ell(\overline{g}_\ell)\,[1 - \eta^\text{m}]\,, \tag{3.18}$$

where we used the matching condition $\overline{g}_\ell(m_*/\Lambda_\ell) = \overline{g}_\ell(m_*/(P\Lambda))$. Combined with the straightforward derivative of the right hand side we can solve for η^m and obtain

$$\eta^\text{m} = 1 - \frac{\beta_\text{f}(g_*)}{\beta_\ell(g_*\,\widetilde{C}(g_*))}\left[\widetilde{C}(g_*) + g_*\frac{\text{d}}{\text{d}g_*}\widetilde{C}(g_*)\right], \quad \widetilde{C}(x) = \sqrt{C(x)}\,, \tag{3.19}$$

where we used eq. (3.15) to replace $\overline{g}_\ell = g_*\,\widetilde{C}(g_*)$. Finally, with $\frac{M}{m_*}\frac{\partial m_*}{\partial M} = (1 - \tau_\text{f}(g_*))^{-1}$, (see e.g. [17], section 3.3.2) we derive

$$\eta^\text{M} = \frac{\eta^\text{m}}{1 - \tau_\text{f}(g_*)}\,. \tag{3.20}$$

The first terms in the perturbative expression

$$\eta^\text{m} = \eta_0 + \eta_1 g_*^2 + \eta_2 g_*^4 + \eta_3 g_*^6 + \eta_4 g_*^8 + \dots \tag{3.21}$$

are given by

$$\eta_0 = 1 - \frac{b_0(N_\text{f})}{b_0(N_\ell)} > 0\,, \quad \eta_1 = (\eta_0 - 1)\left[\tilde{b}_1(N_\text{f}) - \tilde{b}_1(N_\ell)\right], \tag{3.22}$$

with $\tilde{b}_i(N_\text{f}) = b_i(N_\text{f})/b_0(N_\text{f})$. The flavor dependence of the coefficients of the QCD β-function (3.3) is made explicit here. The perturbative expansion of η^M

$$\eta^\text{M} = \eta_0 + \eta_1^\text{M} g_*^2 + \eta_2^\text{M} g_*^4 + \eta_3^\text{M} g_*^6 + \eta_4^\text{M} g_*^8 + \dots\,, \tag{3.23}$$

is obtained from (3.20) and the coefficients are given by the recursion

$$\eta_i^\text{M} = \eta_i - \sum_{j=0}^{i-1} d_j\,\eta_{i-1-j}^\text{M}\,. \tag{3.24}$$

For example $\eta_1^\text{M} = \eta_1 - d_0\eta_0$, where d_0 is the universal coefficient of the QCD anomalous dimension (3.6). The higher order coefficients η_i, up to $i = 4$, are collected in appendix A.

Table 1
Numerical size of the perturbative coefficients in eqs. (3.21), (3.23) and (3.26).

N_f	N_ℓ	η_0	η_1	η_1^M	$\eta_1^M/2b_0(N_f)$	$\log(k)$
2	0	0.121212	0.007467	0.001326	0.010829	0.046655
5	3	0.148148	0.011154	0.003648	0.037574	0.017501
4	3	0.074074	0.005577	0.001824	0.017284	0.012756
5	4	0.080000	0.006505	0.002452	0.025252	0.002622

We note that for fixed N_ℓ the first two coefficients are exactly proportional to $N_f - N_\ell$

$$\eta_0 = \frac{2(N_f - N_\ell)}{33 - 2N_\ell}, \quad \eta_1 = \frac{642(N_f - N_\ell)}{(4\pi)^2(33 - 2N_\ell)^2}, \quad \eta_1^M = \frac{2(57 + 16N_\ell)(N_f - N_\ell)}{(4\pi)^2(33 - 2N_\ell)^2}. \tag{3.25}$$

At higher orders this is only true up to small corrections. The dependence on N_ℓ at fixed $N_f - N_\ell$ is weak and amounts to a difference of about 20% at leading order between $N_\ell = 0$ and $N_\ell = 3$. In Table 1 we list numerical values for interesting combinations of N_f and N_ℓ.

Integrating eq. (3.12) now gives an asymptotic expression for the mass dependence of non-perturbative low energy scales $\mathcal{S}_f$ from perturbation theory ($L_M = \log(M/\Lambda)$)

$$P = \frac{1}{k}\exp(\eta_0 L_M)\,(L_M)^{\eta_1^M/(2b_0(N_f))} \times \left[1 + O\left(\frac{\log(L_M)}{L_M}\right)\right], \tag{3.26}$$

where the constant k is fixed by the conventions for the Λ-parameter and the RGI mass M, which we specified at the beginning of the section, to:

$$\log(k) = \frac{\tilde{b}_1(N_f)}{2b_0(N_f)}\log(2) - \frac{\tilde{b}_1(N_\ell)}{2b_0(N_\ell)}\log(2b_0(N_f)/b_0(N_\ell)). \tag{3.27}$$

See Appendix B for the derivation of eq. (3.26). We note that the leading correction in the expansion eq. (3.26) is $\log(L_M)/L_M$. It contains a term $g_*^2\log(g_*^2)$, cf. eq. (B.5), which makes the convergence of the expansion slow. Therefore for the numerical evaluation of P we prefer to use the formula eq. (3.28) which has corrections only in powers of g_*^2 (no logarithms), see the details in section 3.3. Accidentally, for the interesting cases, the asymptotic expression eq. (3.26) for P is dominated by $\exp(\eta_0 L_M) = (M/\Lambda)^{\eta_0}$. This can be seen by the numerical smallness of $\eta_1^M/2b_0(N_f)$ and $\log(k)$ in Table 1.

3.3. Accuracy of perturbation theory

A consistency check on the applicability of perturbation theory is the comparison of different orders. Indeed, Figs. 1–3 show that higher orders do not contribute very much, in particular when one uses the mass dependence in terms of the RGI mass, η^M. This also suggests that it is an advantage to consider the perturbative prediction for P in terms of M/Λ instead of working with m_*/Λ. We have worked with M/Λ in [11] and will do so below in our comparison to a non-perturbative investigation.

Details for η^m and η^M are seen in Figs. 1–3. In the legends of the plots the number of loops corresponds to the highest loop order of the β function which is used. We note that in the right plot of Fig. 2 the 5-loop correction is larger in magnitude than the 4-loop correction for $g^2 \gtrsim 3$. But the corrections are amazingly small.

Renormalization group improved perturbative predictions for the function $P(M/\Lambda) = \Lambda_\ell/\Lambda_f$ can be obtained from (cf. eq. (3.1))

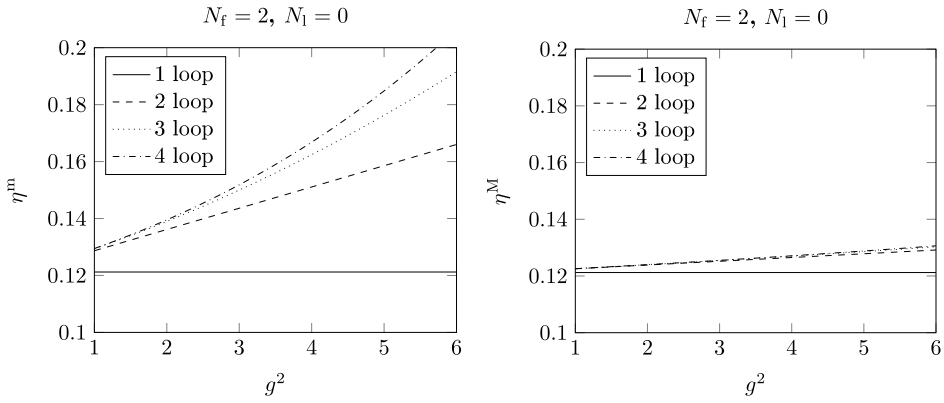

Fig. 1. The functions $\eta^\mathrm{m}(g^2)$, $\eta^\mathrm{M}(g^2)$ for the case $N_\mathrm{f} = 2$, $N_\ell = 0$. The number of loops corresponds to the highest loop order of the β function which is used.

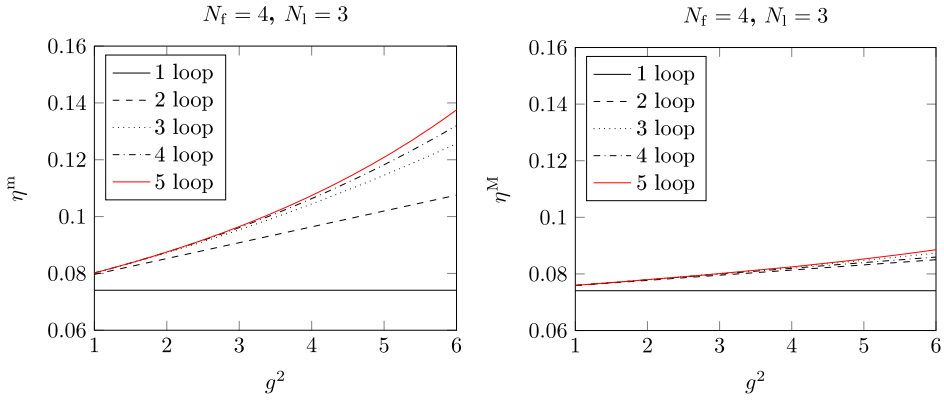

Fig. 2. The functions $\eta^\mathrm{m}(g^2)$, $\eta^\mathrm{M}(g^2)$ for the case $N_\mathrm{f} = 4$, $N_\ell = 3$. The number of loops corresponds to the highest loop order of the β function which is used.

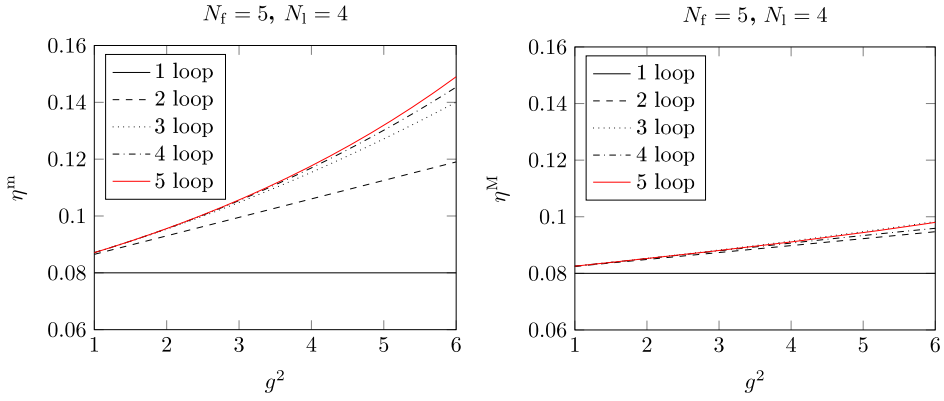

Fig. 3. The functions $\eta^\mathrm{m}(g^2)$, $\eta^\mathrm{M}(g^2)$ for the case $N_\mathrm{f} = 5$, $N_\ell = 4$. The number of loops corresponds to the highest loop order of the β function which is used.

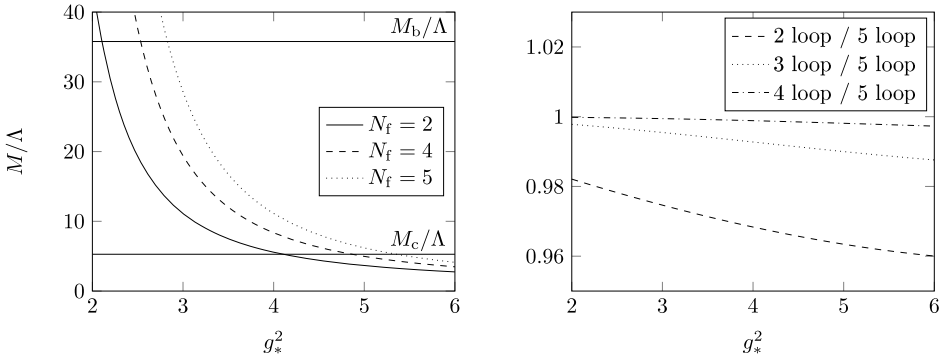

Fig. 4. Left: The relation between M/Λ and g_* at 5-loop. Right: The 2, 3 and 4-loop relation divided by the 5-loop one for the case of $N_f = 2$, $N_\ell = 0$.

$$P(M/\Lambda) = \exp\left\{ I_g^\ell(g_* \widetilde{C}(g_*)) - I_g^f(g_*) \right\}, \tag{3.28}$$

where

$$\exp(I_g^i(\bar{g})) = \left(b_0(N_i)\bar{g}^2\right)^{-b_1(N_i)/(2b_0(N_i)^2)} \mathrm{e}^{-1/(2b_0(N_i)\bar{g}^2)} \tag{3.29}$$

$$\times \exp\left\{ -\int_0^{\bar{g}} \mathrm{d}x \left[\frac{1}{\beta_i(x)} + \frac{1}{b_0(N_i)x^3} - \frac{b_1(N_i)}{b_0(N_i)^2 x} \right] \right\} . \tag{3.30}$$

The coupling $g_* = \bar{g}(m_*)$ is obtained from inverting

$$\frac{\Lambda}{M} = \frac{\left(b_0\bar{g}^2\right)^{-b_1/(2b_0^2)}}{(2b_0\bar{g}^2)^{-d_0/(2b_0)}} \mathrm{e}^{-1/(2b_0\bar{g}^2)} \exp\left\{ -\int_0^{g_*(M/\Lambda)} \mathrm{d}x \left[\frac{1-\tau_f(x)}{\beta_f(x)} + \frac{1}{b_0 x^3} - \frac{b_1}{b_0^2 x} + \frac{d_0}{b_0 x} \right] \right\}, \tag{3.31}$$

where M is the RGI mass corresponding to m_*. For this equation we have combined eqs. (3.1) and (3.4) using $\mu = \overline{m} = m_*$. For reference the resulting relation is plotted in the left panel of Fig. 4 together with the values for M_c/Λ and M_b/Λ which were obtained from the PDG values [18] for $\overline{m}_c/\Lambda$ and $\overline{m}_b/\Lambda$, and inverting eq. (3.1). Of course, in case of the charm quark $N_f = 4$ and in the case of the bottom quark $N_f = 5$ were used.

The predictions for different orders of perturbation theory are very close to the unsystematic one-loop "approximation", $P^{(1)} = (M/\Lambda)^{\eta_0}$, as long as $M/\Lambda < 30$ or so and the number of flavors is small. This is accidental. In Figs. 5–7 we plot the one-loop "approximation" and the 4-loop result on the left and the relative correction

$$(P - P^{(1)})/P^{(1)} \tag{3.32}$$

at 2,3,4-loop on the right. When it is available we also add the 5-loop result. In this comparison, when we consider at least 2-loop precision, we always work to a consistent order in the renormalization group functions. Note that we truncate the renormalization group functions β, τ in the integrals eq. (3.30), eq. (3.31) and 2-loop accuracy means, e.g.,

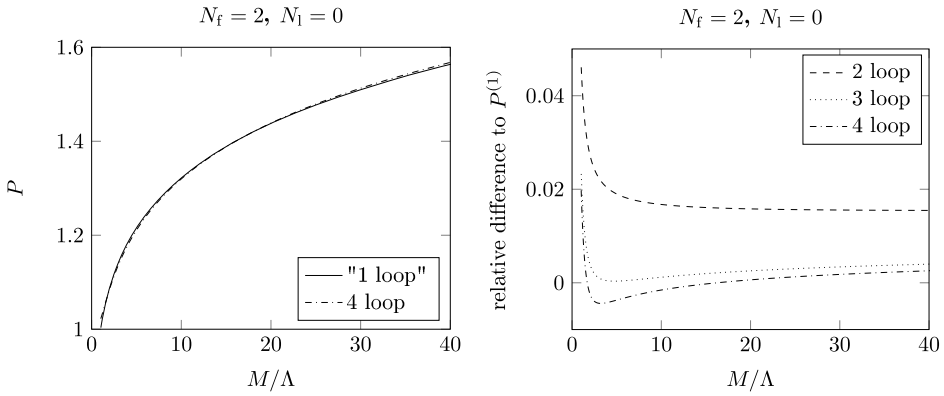

Fig. 5. The mass-dependence P at 1-loop formula and at 4-loop (left) as well as 2,3,4-loop correction normalized to the 1-loop approximation (right) for the case $N_f = 2$, $N_\ell = 0$.

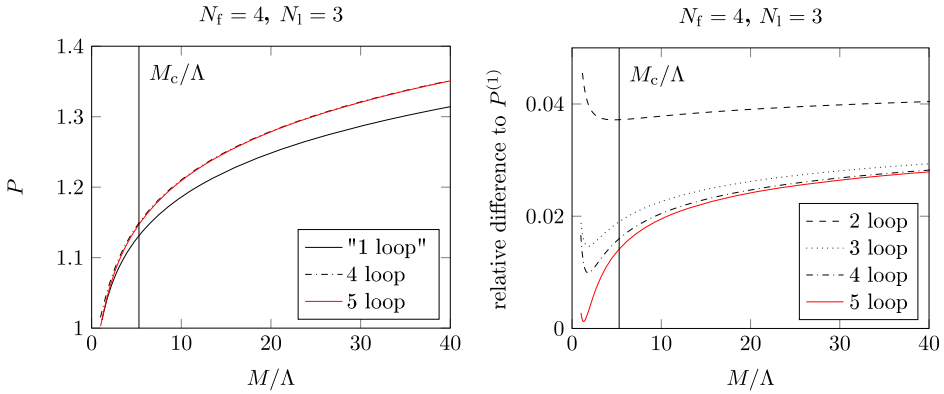

Fig. 6. The mass-dependence P at 1-loop formula and at 4,5-loop (left) as well as 2,3,4,5-loop correction normalized to the 1-loop approximation (right) for the case $N_f = 4$, $N_\ell = 3$.

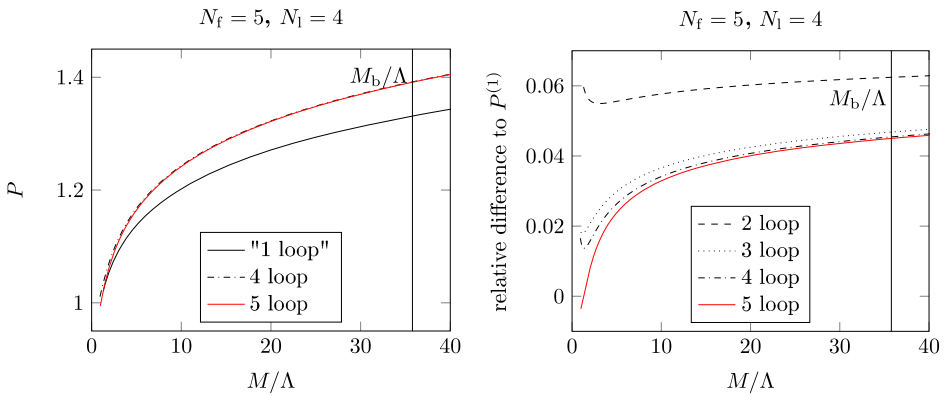

Fig. 7. The mass-dependence P at 1-loop formula and at 4,5-loop (left) as well as 2,3,4,5-loop correction normalized to the 1-loop approximation (right) for the case $N_f = 5$, $N_\ell = 4$.

Table 2
Perturbative values of $P_{\ell,\mathrm{f}}$ defined in eq. (3.9) for various cases of interest, see main text for details.

N_f	N_ℓ	1 loop	2 loop	3 loop	4 loop	5 loop
2	0	1.2319	1.2546	1.2170	1.2084	-
4	3	1.1448	1.1875	1.1552	1.1492	1.1468
5	4	1.3413	1.4255	1.3947	1.3918	1.3913

$$\frac{1-\tau(x)}{\beta(x)} = -\frac{1}{x^3}\left[\frac{1}{b_0+b_1x^2}+x^2\frac{d_0}{b_0}\right]. \tag{3.33}$$

The function $C(g)$ only enters at 3-loop precision since $c_1 = 0$. It is only needed for the upper integration limit in eq. (3.28) and there we compute explicitely $\widetilde{C}(g_*) = \sqrt{C(g_*)}$.

In the numerical results we observe in particular that for the phenomenologically relevant case of $N_\mathrm{f} = 5$, $N_\ell = 4$, the 3-loop contribution (difference 3-loop to 2-loop) is around 2% while the 4- and 5-loop ones are then nice and small, see the right plot in Fig. 7. Judging by perturbation theory alone, the perturbative prediction for decoupling the b-quark should be very reliable. Also for the other phenomenologically relevant case of decoupling the c-quark ($N_\mathrm{f} = 4$, $N_\ell = 3$) perturbation theory appears to work quite well.

These curves suggest that perturbative decoupling introduces only errors at the sub-percent level for the ratios of Lambda parameters, once perturbation theory applies at all. In Table 2 we list the values of P computed from eq. (3.28) using different orders of perturbation theory. We evaluate P at an argument M/Λ which depends on N_f and N_ℓ. For $N_\mathrm{f} = 2$, $N_\ell = 0$ we obtain M/Λ from the PDG value for $\overline{m}_\mathrm{c}$ [18] and $\Lambda_2 = 310$ MeV from [19]. In this case there is no 5-loop result because the coefficient c_4 is not known. For $N_\mathrm{f} = 4$, $N_\ell = 3$ and $N_\mathrm{f} = 5$, $N_\ell = 4$ we use the PDG values for M_c/Λ and M_b/Λ as explained above.

4. Non-perturbative investigation for $N_\mathrm{f} = 2 \to N_\ell = 0$

We investigate a model, namely QCD with $N_\mathrm{f} = 2$ heavy, mass-degenerate quarks. The decoupling is then $2 \to 0$ and the Lagrangian of the effective theory, $\mathcal{L}_\mathrm{dec}$, is the Yang-Mills one up to $1/M^2$ corrections. We target the RGI quark mass values (see below)

$$\frac{M_\mathrm{targ}}{\Lambda} = 0.59\,,\ 1.28\,,\ 2.50\,,\ 4.87\,,\ 5.7781\,. \tag{4.1}$$

Using $\Lambda \equiv \Lambda_2 = 310\,\mathrm{MeV}$ from [19] their physical values are approximately M_targ =0.2, 0.4, 0.8, 1.5, 1.8 GeV. The value $M_\mathrm{targ}/\Lambda = 4.87$ corresponds to the RGI charm quark mass M_c from [20] in agreement with [18] within the present uncertainties. However, for our model study the exact value is not important.

4.1. Low energy observables

In principle any low-energy hadronic scale $\mathcal{S}(M)$ can be used to study decoupling, but in practice some choices are far superior to others. Ideally we look for a quantity that is easily non-perturbatively renormalizable, well defined in both full and effective theory, has controllable lattice artifacts, is cheap to compute and can be determined with a high precision. Since in our case the effective theory has no fermionic content, we are restricted to purely gluonic observables. Glueball masses would be natural candidates. However, it is difficult to determine them precisely

enough. Hadronic scales derived from the static quark potential fulfill all criteria and have been popular for many years. If $F(r)$ denotes the force between two static quarks (defined in terms of the fundamental Wilson loop), a distance r_x can be defined implicitly [13] by choosing a number c and solving

$$r_x^2 F(r_x) = c\,. \tag{4.2}$$

The choices $r_0 \Leftrightarrow c = 1.65$ [13] and $r_1 \Leftrightarrow c = 1.0$ [21] have become standards. In a lattice calculation the latter has a better statistical precision, but larger lattice artifacts. Moreover we expect decoupling to be more precise for the longer distance, r_0.

In recent years, these scales have been largely replaced by scales based on the gradient flow [1,22]. The gauge field A_μ is used as an initial condition in a flow equation, that describes the relaxation of a field B_μ as a function of a flow time t.

$$\partial_t B_\mu = D_\nu G_{\nu\mu}\,, \qquad B_\mu\big|_{t=0} = A_\mu\,. \tag{4.3}$$

The field strength tensor $G_{\nu\mu}$ and the covariant derivative D_ν are defined in the usual way, but at flow time t. The crucial observation, that correlators of the B_μ fields at finite flow time are renormalized quantities [23], allowed to introduce a family of scales. The definition of scales $\sqrt{t_0}$ [1], $\sqrt{t_c}$ and w_0 [14] is based on the dimensionless combination

$$\mathcal{E}(t) = t^2 \left\langle \frac{1}{4} G^a_{\mu\nu} G^a_{\mu\nu} \right\rangle, \tag{4.4}$$

together with

$$\mathcal{E}(t_0) = 0.3\,, \tag{4.5}$$

$$\mathcal{E}(t_c) = 0.2\,, \tag{4.6}$$

$$w_0^2 \mathcal{E}'(w_0^2) = 0.3\,. \tag{4.7}$$

In our simulations we compute the hadronic scales

$$\mathcal{S}(M) = \frac{1}{r_0}\,,\ \frac{1}{\sqrt{t_0}}\,,\ \frac{1}{\sqrt{t_c}}\,,\ \frac{1}{w_0}\,. \tag{4.8}$$

The rest of this section contains technical details about the lattice simulations. It can be omitted if one is only interested in the physical results presented in section 5.

4.2. Fixing the RGI parameters of the theory and details of the simulations

4.2.1. Discretization

We use Wilson's plaquette gauge action [24] and include quarks treated with two discretizations: O(a) improved Wilson fermions [25,26] and twisted mass [27] Wilson fermions at maximal twist. For both actions the clover term [25,26] has the non-perturbatively determined improvement coefficient $c_{\rm sw}$ [28]. Twisted mass fermions at maximal twist are automatically O(a) improved [29] also without a clover term. However, with the clover term added our two discretizations have a common chiral limit in a finite volume (see L_1 below). Furthermore the clover term reduces O(a^2) lattice artifacts as it was shown for example in [30].

In appendix C we list the ensembles generated with standard Wilson fermions in Table 4 and with twisted mass Wilson fermions in Table 5. The twisted mass simulations are the same as in [31].

We determine the lattice spacings through the scale L_1 [19,32], which is defined by $\bar{g}^2_{\rm SF}(L_1) = 4.484$ through the so-called Schrödinger Functional coupling at zero quark mass and in a finite volume of size L_1^4. Note that in this situation the two discretizations are identical. Thus at a given gauge coupling $\beta = 6/g_0^2$ they have one and the same lattice spacing. The values of L_1/a and the corresponding lattice spacings are listed in Table 6.

4.2.2. O(a) improvement and finite size effects

O(a) improvement of quark mass effects requires to keep the improved bare coupling $\tilde{g}_0^2 = (1 + b_{\rm g}(N_{\rm f})\, am_{\rm q})\, g_0^2$ fixed, where $m_{\rm q} = 1/(2\kappa) - 1/(2\kappa_{\rm c})$ is the bare subtracted standard mass. Twisted mass fermions at maximal twist have $m_{\rm q} = 0$ and therefore the improved coupling is $\tilde{g}_0 = g_0$. Instead our simulations with standard Wilson fermions were done at fixed g_0 (and not $\tilde{g}_0$). We correct for the resulting O(am) effects in the lattice spacing by decreasing the values of $a\mathcal{S}(M)$ using the 1-loop result $b_{\rm g}(N_{\rm f}) = 0.01200\, N_{\rm f}\, g_0^2$ [33,34] and the 1-loop β-function. For $\mathcal{S} = 1/\sqrt{t_0(M)}$ these effects shift the value of $\sqrt{t_0(M)}/a$ according to

$$\left.\frac{\sqrt{t_0(M)}}{a}\right|_{\tilde{g}_0} \approx \left.\frac{\sqrt{t_0(M)}}{a}\right|_{g_0} \times \left[1 + \frac{0.01200\, N_{\rm f}}{2b_0(N_{\rm f})}\, am_{\rm q}\right]. \tag{4.9}$$

We use $am_{\rm q} = am/(Zr_{\rm m})$ and the factor $Zr_{\rm m}$ is taken from [19] (at $6/g_0^2 = 5.7$ we get $Zr_{\rm m} = 1.194$ from a Padé fit). Here am denotes the PCAC mass. We added in quadrature 100% of the correction to the errors as an estimate of unknown O(g_0^4) terms in $b_{\rm g}$. After the corrections the values of $a\mathcal{S}(M)$ correspond to simulations performed at $\beta = 6/\tilde{g}_0^2$.

Our volumes are such that the lightest pseudo-scalar mass times the box size is $m_{\rm PS}L \geq 7.4$ and $L/\sqrt{t_0(M)} \geq 12$ and $L/r_0(M) \geq 3.8$. At our largest masses the situation is comparable to the pure gauge theory, where significant finite volume effects can be excluded for a lattice size $L \approx 4r_0 = 2.0$fm. Approximate decoupling of the heavy quarks means that also our finite mass simulations are practically free of finite volume effects.

4.2.3. Quark masses

Before taking the continuum limit, we non-perturbatively fix the value of the RGI quark mass M in units of the Λ parameter through the following steps. We take the Λ parameter to be defined in the $\bar{\rm MS}$ scheme while the RGI mass M is independent of the scheme.

In the case of standard Wilson fermions the renormalized quark mass in lattice units $a\overline{m}_{\rm SF}(L_1)$ at length scale L_1 is defined by $a\overline{m}_{\rm SF}(L_1) = Z_{\rm A}/Z_{\rm P}(L_1)\, am$, where the renormalization factor $Z_{\rm P}(L_1)$ is defined in the Schrödinger Functional scheme as in [19] and also the details of the definition of m are found there. The axial current renormalization factor, $Z_{\rm A}$, is fixed by a chiral Ward identity [35].[2] For the determination of the PCAC mass am we use our publicly available program.[3] The ratio M/Λ is then obtained from

$$\frac{M}{\Lambda} = a\overline{m}_{\rm SF}(L_1) \times M/\overline{m}_{\rm SF}(L_1) \times \frac{(L_1/a)}{(\Lambda L_1)}, \tag{4.10}$$

where we take $M/\overline{m}_{\rm SF}(L_1) = 1.308(16)$ from [19,37] and $\Lambda\, L_1 = 0.649(45)$ from [38]. The values of the PCAC mass m and of M/Λ are tabulated in Table 4. The accuracy of M/Λ is around

[2] A more precise determination of $Z_{\rm A}$ became recently available [36].

[3] It is available at https://github.com/to-ko/mesons.

7% with an error dominated by the one of ΛL_1. Thus, ratios of masses M_1/M_2 or equivalently logarithmic derivatives with respect to masses are known significantly more precisely.

In the case of twisted mass fermions at maximal twist the difference is that the renormalized quark mass $a\overline{m}_{\rm SF}(L_1)$ is calculated through $a\overline{m}_{\rm SF}(L_1) = a\mu/Z_{\rm P}(L_1)$, where $a\mu$ is the twisted mass parameter. The ratio M/Λ is again obtained from eq. (4.10). For twisted mass fermions we actually invert eq. (4.10) to determine the twisted mass parameter corresponding to given values of M/Λ which are tabulated in Table 5.

4.2.4. Hadronic scales on the lattice

In our simulations we measure the observables discussed in section 4.1. Various details concerning their computation in the discretized theory are as follows.

The clover (symmetric) definition of the action density E is used in eq. (4.4) and we use the Wilson-flow equation, cf. [1].

The scale r_0 is defined with the "HYP2" action for the static quarks [39]. It is determined with our publicly available program[4] following the details explained in Ref. [40]. We use a variational basis with up to four levels of spatial HYP smearing [41] to construct a matrix of Wilson loops. Due to the open boundary conditions, Wilson loops are averaged only in a temporal region sufficiently far away from the boundaries to exclude contaminations from boundary effects. The static potential as a function of r is obtained by solving the generalized eigenvalue problem as discussed in Ref. [40].

Hadronic scales such as t_0 are non-linear functions of one or more Monte-Carlo averages of "primary observables" $\langle\mathcal{O}_1\rangle, \ldots, \langle\mathcal{O}_{N_{\rm ob}}\rangle$, like for instance the action densities at different flow times. The derivative of such a function with respect to the twisted mass, as needed for the MC evaluation of $\eta^{\rm M}$ (below in eq. (5.6)), is in general given by

$$\frac{\mathrm{d}f(\langle\mathcal{O}_1\rangle, \ldots, \langle\mathcal{O}_{N_{\rm ob}}\rangle, \mu)}{\mathrm{d}\mu} = \sum_{i=1}^{N_{\rm ob}} \frac{\partial f}{\partial\langle\mathcal{O}_i\rangle}\frac{\mathrm{d}\langle\mathcal{O}_i\rangle}{\mathrm{d}\mu} + \frac{\partial f}{\partial\mu} \tag{4.11}$$

and the derivative of a primary observable $\mathcal{O}$,

$$\frac{\mathrm{d}\langle\mathcal{O}\rangle}{\mathrm{d}\mu} = -\left\langle\frac{\mathrm{d}S}{\mathrm{d}\mu}\mathcal{O}\right\rangle + \left\langle\frac{\mathrm{d}S}{\mathrm{d}\mu}\right\rangle\langle\mathcal{O}\rangle + \left\langle\frac{\mathrm{d}\mathcal{O}}{\mathrm{d}\mu}\right\rangle. \tag{4.12}$$

For most observables $\frac{\partial f}{\partial\mu}$ and $\frac{\mathrm{d}\mathcal{O}}{\mathrm{d}\mu}$ are absent. The derivative of the action is given by $\mathrm{d}S/\mathrm{d}\mu = ia^4\sum_x \bar\psi(x)\gamma_5\tau^3\psi(x)$. In cases like ours, where the observables do not contain fermionic fields, no new Wick contractions arise in the first term, and one simply needs to determine the observable and the action-derivative on each configuration and compute their connected correlation. For the action-derivative we write (cf. [42])

$$\begin{aligned}\left\langle\frac{\mathrm{d}S}{\mathrm{d}\mu}\right\rangle &= ia^4\sum_x\left\langle\mathrm{tr}\left[(D_d(x,x)^{-1} - D_u^{-1}(x,x))\gamma_5\right]\right\rangle^{\rm gauge}\\ &= -2\mu a^8\sum_{x,y}\left\langle\mathrm{tr}\left[D_u^{-1\dagger}(x,y)D_u^{-1}(x,y)\right]\right\rangle^{\rm gauge},\end{aligned} \tag{4.13}$$

where in the last step a property of the twisted mass Dirac operators $D_{u,d}$ (for up and down quark), $D_u - D_d = 2i\gamma_5\mu$, was exploited, leading to an expression that has a smaller variance,

[4] It is available at https://github.com/bjoern-leder/wloop.

when the trace is estimated stochastically. A stochastic estimation is necessary to avoid a full matrix inversion, and amounts to solving equations $D_u\xi = \eta$, with 4D noise spinors η, for ξ and a subsequent dot product $\xi \cdot \xi$. We find that different noise distributions (e.g. normal or $U(1)$-noise) yield a similar variance, and further refinements like spin or color dilution [43] do not pay off. Not many noise-sources are needed for the final error to be close to the limiting error due to gauge field fluctuations. In our measurements we settle for 64 $U(1)$ noise spinors per configuration.

4.2.5. Simulation algorithms

In the case of standard Wilson fermions, part of the simulations are performed using periodic boundary conditions (except for anti-periodic boundary conditions in temporal direction for the fermions) and the MP-HMC algorithm [44]. In order to avoid the freezing of the topological charge (see also next section), for simulations with $t_0/a^2 > 5.5$ [45,46] we adopt open boundary conditions in time and use the publicly available openQCD package[5] [47]. We set the boundary improvement coefficients to their tree-level values $c_{\rm G} = 1$ and $c_{\rm F} = 1$. In both cases the fermion determinant is Hasenbusch-factorized [48] using a splitting in two factors, thus two pseudo-fermion fields are needed and a hierarchical numerical integrator is employed (Leapfrog and Omelyan-Mryglod-Folk integrator schemes are used at the different levels). The trajectory length is always set to 2.0 and configurations and measurements are separated by at least four trajectories. Most computer resources are spent in the solution of the Dirac equation with the smallest mass. For $M/\Lambda > 1$ we use the SAP preconditioned GCR algorithm [49] while for $M/\Lambda < 1$ it is profitable to use a multigrid solver [50], which is implemented as the two-grid "locally deflated" solver in the openQCD package since version 1.2. The cost of the simulations is low compared to simulations in the chiral regime.

In the case of twisted mass fermions we use a version of openQCD, in which the SAP preconditioner can have a different value of μ than the simulated one. In the preconditioner the twisted mass term is defined only on the even sites. We achieve a significant speed up of the SAP preconditioned GCR algorithm by choosing a value of μ for the SAP preconditioner which is larger by approximately a factor 6 than the simulated one (the multi-grid inverter of [51] implements a similar strategy inspired by our findings).

Open boundary conditions are used as specified above. In this setup the Wilson–Dirac operator has two mass parameters, the standard bare quark mass m_0 and the twisted mass μ. Maximal twist means that m_0 is set to its critical value m_c which corresponds to the vanishing of the current (PCAC) quark mass. We extracted the critical mass from Table 13 in [19], interpolating the data to the desired β values by a Padé fit in $g_0^2 = 6/\beta$ of the form

$$am_c(g_0) = u_1\, g_0^2 + g_0^4\, \frac{\sum_{k=0}^{3} u_{2+k}\, g_0^{2k}}{1 + u_d\, g_0^2} \tag{4.14}$$

where the coefficients u_1 and u_2 coincide with two-loop perturbation theory [52]. The values of the hopping parameter $\kappa = 1/(2am_c + 8)$ are listed in Table 5.

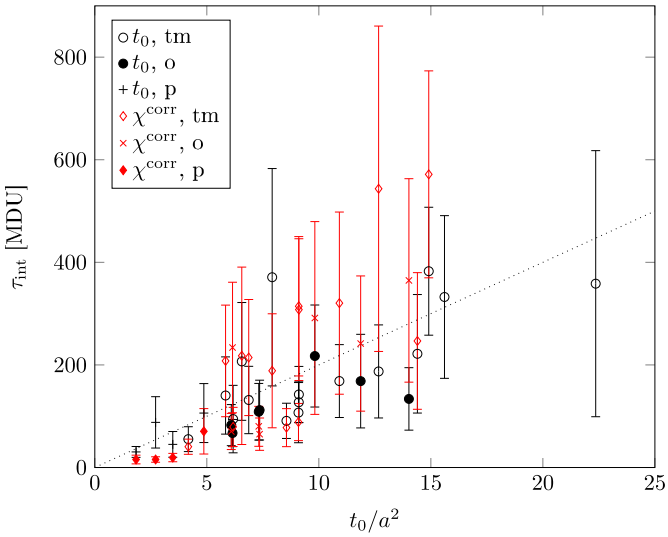

Fig. 8. Autocorrelation times derived from observables which are expected to have large overlap with the slowest modes in the simulation are plotted as a function of $t_0(M)/a^2$. The dotted line represents eq. (4.15).

4.2.6. Autocorrelation times and error analysis

We measure the integrated autocorrelation time τ_{int} for all measured quantities including the hadronic scales, the PCAC mass and additionally the topological susceptibility. We find the largest τ_{int} for the scale t_0 and for the topological susceptibility χ^{corr} as defined in [46], see Fig. 8, which we use as a rough estimate of the exponential autocorrelation time τ_{exp}, cf. [45].

At the smallest lattice spacing $a = 0.036\,\mathrm{fm}$ that we reach with standard Wilson fermions we estimate $\tau_{\mathrm{exp}} \simeq 200 - 300$ MDU (Molecular Dynamics Units). Our statistics of $4000 - 8000$ MDU is therefore adequate but does require a particularly careful error analysis. With twisted mass fermions at maximal twist we reach a smallest lattice spacing of $a = 0.023\,\mathrm{fm}$ ($\beta = 6.0$). There we estimate $\tau_{\mathrm{exp}} = 357$ MDU and have a statistics of $63\tau_{\mathrm{exp}}$. For the twisted mass simulations at $M/\Lambda = 4.87$ and $\beta = 5.88\,,\ 6.0$ the statistics is too small to determine τ_{int} for χ^{corr}. The autocorrelation times shown in Fig. 8 are reasonably well described by the dotted line

$$\tau_{\mathrm{exp}} = 20 t_0/a^2\,, \tag{4.15}$$

where one has to take into account that determinations of τ_{exp} including an error estimate are notoriously difficult. Thus the data in Fig. 8 is consistent with the expectation, that for simulations with open boundary conditions autocorrelation times scale with $1/a^2$.

The error analysis is performed with the program[6] of [45]. It is based on [53] and adds a tail to the autocorrelation function as an estimate of the slow mode contribution [45].

[5] http://luscher.web.cern.ch/luscher/openQCD/.
[6] http://www-zeuthen.desy.de/alpha/.

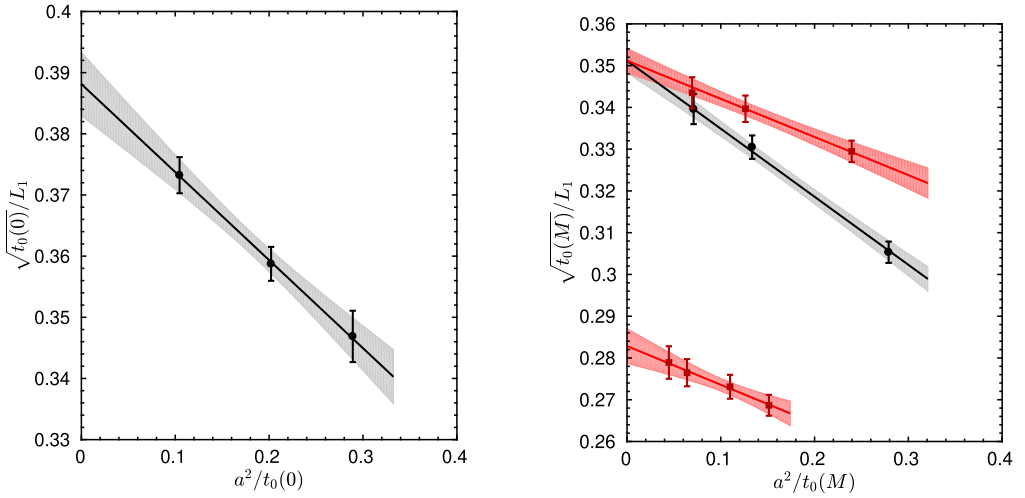

Fig. 9. Continuum extrapolations of $\sqrt{t_0}/L_1$, using a linear extrapolation in a^2/t_0. The shaded bands are the extrapolation errors. The left plot shows the results for $\sqrt{t_0(0)}$ in the chiral limit. The right plot shows the results for $\sqrt{t_0(M)}$ at $M/\Lambda = 0.59$ (upper data set in the plot) and $M/\Lambda = 4.87$ (the charm quark mass M_c, lower data set in the plot). Black circles represent the standard Wilson and red squares the twisted mass discretizations. Where both are available a combined continuum extrapolation is performed.

5. Non-perturbative mass dependence

5.1. Test of the factorization formula

We remind that our model is QCD with two heavy, mass-degenerate quarks and thus the effective theory, decQCD, is the Yang-Mills theory up to $1/M^2$ corrections ($N_f = 2$, $N_\ell = 0$). For the hadronic scale $\mathcal{S} = 1/\sqrt{t_0}$ [1], the factorization formula eq. (3.10) takes the form

$$\sqrt{\frac{t_0(M)}{t_0(0)}} = \frac{1}{Q_{0,2}^{1/\sqrt{t_0}} \times P_{0,2}(M/\Lambda)} + \mathrm{O}((\Lambda/M)^2) \tag{5.1}$$

with $Q_{0,2}^{1/\sqrt{t_0}} = [\Lambda\sqrt{t_0(0)}]_{N_f=2}/[\Lambda\sqrt{t_0}]_{N_f=0}$. We turn now to a comparison of eq. (5.1) to non-perturbative data. Preliminary results have been presented in [54], where only data for Wilson fermions were available. Now we can combine those data with the new simulations with twisted mass fermions and perform careful continuum extrapolations. In the extrapolations we only use data points which satisfy $a^2/t_0(M) < 0.32$.

In order to compute the ratio in eq. (5.1) we write

$$\sqrt{\frac{t_0(M)}{t_0(0)}} = \frac{\sqrt{t_0(M)}}{L_1} \times \left(\frac{\sqrt{t_0(0)}}{L_1}\right)^{-1} \tag{5.2}$$

and separately take continuum limits for the two factors on the right hand side. There the mass independent scale L_1 enters, see section 4. The pairs $(L_1/a\,,\ \beta)$ are computed from a quadratic fit of $\ln(L_1/a)$ as a function of β. We take data for L_1/a from Table 13 of [19] and add the newly determined values $L_1/a = 20.31(69)$ at $\beta = 6.1569$ and $L_1/a = 24.83(88)$ at $\beta = 6.2483$.

Table 3
The values of $\sqrt{t_0(M)/t_0(0)}$ computed through eq. (5.2). The errors are obtained from error propagation which takes into account the correlation between the two factors in eq. (5.2).

M/Λ	$\sqrt{t_0(M)/t_0(0)}$
0.5900	0.9048(43)
1.2800	0.8458(74)
2.5000	0.7880(73)
4.8700	0.7287(127)
5.7781	0.7151(102)

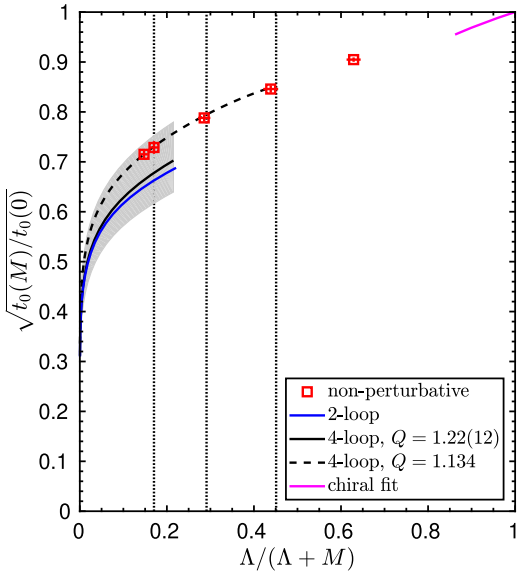

Fig. 10. The mass-dependence of the ratio $\sqrt{t_0(M)/t_0(0)}$ in the theory with two mass-degenerate quarks. Monte Carlo data after continuum extrapolation are compared with the perturbative predictions for $1/(QP)$ at large M eq. (5.1). The gray shaded error band represents the error of the 4-loop curve (black line) deriving from Q. The dashed line is the 4-loop curve adjusting the value of Q to go through the point at $M/\Lambda = 5.7781$, see eq. (5.4). A fit function which describes the mass-dependence close to the chiral limit is also shown to the right. The vertical dotted lines mark the values of the quark mass M_c, $M_c/2$ and $M_c/4$. (For interpretation of the colors in the figure(s), the reader is referred to the web version of this article.)

The first factor on the right hand side of eq. (5.2) is computed using the data $t_0(M)/a^2$ obtained in the simulations listed in Table 4 and Table 5. For the simulations with standard Wilson fermions we include the b_g effects as explained in section 4.2.2. We have data for five values of the quark masses given in eq. (4.1). Some of our data for the ratio $\sqrt{t_0(M)}/L_1$ are shown in the right plot of Fig. 9 together with their continuum extrapolations. We show the two extreme values of the quark mass, separated by a factor of 8. The extrapolations linear in a^2/t_0 work very well and we observe that the size of cut-off effects is smaller for the twisted mass data. For this reason we opted for the twisted mass discretization to simulate masses at or larger than the charm quark mass.

In order to compute the second factor on the right hand side of eq. (5.2) we use the values of $t_0(0)/a^2$ in the chiral limit which are known for $\beta = 6/g_0^2 = 5.2$, 5.3 and 5.5 from [55]. The continuum extrapolation of $\sqrt{t_0}(0)/L_1$ linear in $a^2/t_0(0)$ using the three β values works well, see the left plot of Fig. 9 and yields $\sqrt{t_0(0)}/L_1 = 0.3881(52)$.

Our continuum results for the ratio $\sqrt{t_0(M)/t_0(0)}$ are listed in Table 3. Correlations of the two factors originating from the common data of the scale L_1/a help to reduce the overall error.

Fig. 10 shows the values of $\sqrt{t_0(M)/t_0(0)}$ of Table 3 as a function of $\Lambda/(\Lambda + M)$. We display a horizontal error stemming from the uncertainty of M/Λ originating from ΛL_1 in eq. (4.10). The vertical dotted lines mark the values of the quark mass M_c, $M_c/2$ and $M_c/4$. We compare the Monte Carlo data to the factorization formula eq. (5.1), where the factor $P_{0,2}$ is computed to 2- (blue dashed line) and 4-loops (black line). The error on the factorization formula comes from the numerical values $[\Lambda L_1]_{N_f=2} = 0.629(36)$ [19], $[\sqrt{t_0}/L_1]_{N_f=2} = 0.3881(52)$, $[\Lambda r_0]_{N_f=0} = 0.602(48)$ [56], $[\sqrt{t_0}/r_0]_{N_f=0} = 0.3319(19)$ [31] combined to

$$Q_{0,2}^{1/\sqrt{t_0}} = \frac{[\Lambda L_1]_{N_f=2} \times [\sqrt{t_0(0)}/L_1]_{N_f=2}}{[\Lambda r_0]_{N_f=0} \times [\sqrt{t_0}/r_0]_{N_f=0}} = 1.22(12) \tag{5.3}$$

and is displayed by the gray shaded band only for the 4-loop curve. For completeness, in Fig. 10 the magenta line to the right shows the mass dependence in the chiral limit estimated from [55, 57], cf. [58].

From Fig. 10 we see that there is agreement between the Monte Carlo data of Table 3 and the factorization formula eq. (5.1) for quark masses at the charm quark mass value M_c. Thus within our precision of 10% due to the uncertainty of the factor Q in eq. (5.3), the data match the upper error band of the perturbative prediction. In [11] we presented results for the ratio $r_0(M)/r_0(0)$ and reached similar conclusions albeit with less precise data covering only the region below the charm quark mass. Our new results for $\sqrt{t_0(M)/t_0(0)}$ are much more precise than the value of Q extracted from the literature. This allows to turn the tables and predict

$$Q_{0,2}^{1/\sqrt{t_0}} = 1.134(28)\,, \tag{5.4}$$

obtained by taking $M/\Lambda = 5.7781$ in eq. (5.1). For $\sqrt{t_0(M)/t_0(0)}$ we use our result in the last line of Table 3. We evaluate the factor $P_{0,2}(M/\Lambda = 5.7781) = 1.2328$ and assign to it a conservative 2% error as it will be estimated in section 6. This determination avoids entirely the computation of the running of the coupling at high energy [38,56]. In a nutshell it is replaced by perturbation theory for the difference of the running. The essential point is that the latter is given by the contribution of quark loops for which we non-perturbatively confirm that perturbation theory is very accurate. We will comment more on this in the conclusions.

5.2. *The mass-scaling function* η^{M}

By discretizing the derivative in eq. (3.13) we obtain from our simulations numerical estimates of the mass-scaling function

$$\eta^{\mathrm{M}}(\overline{M}) \approx \frac{\log(\mathcal{S}(M_2)/\mathcal{S}(M_1))}{\log(M_2/M_1)}\,, \quad \overline{M} = \sqrt{M_2 M_1}\,. \tag{5.5}$$

We use this definition to compute $\eta^{\mathrm{M}}(\overline{M})$ at $\overline{M} = \sqrt{1.28 \times 0.59}$ and $\sqrt{2.50 \times 1.28}$ using $\mathcal{S} = 1/\sqrt{t_0}$, $1/\sqrt{t_c}$ and $1/w_0$. As emphasized before, these estimates differ by $1/M^2$ effects. We have data at three values of the lattice coupling $\beta = 6/g_0^2 = 5.3$, 5.5 and 5.7 for both

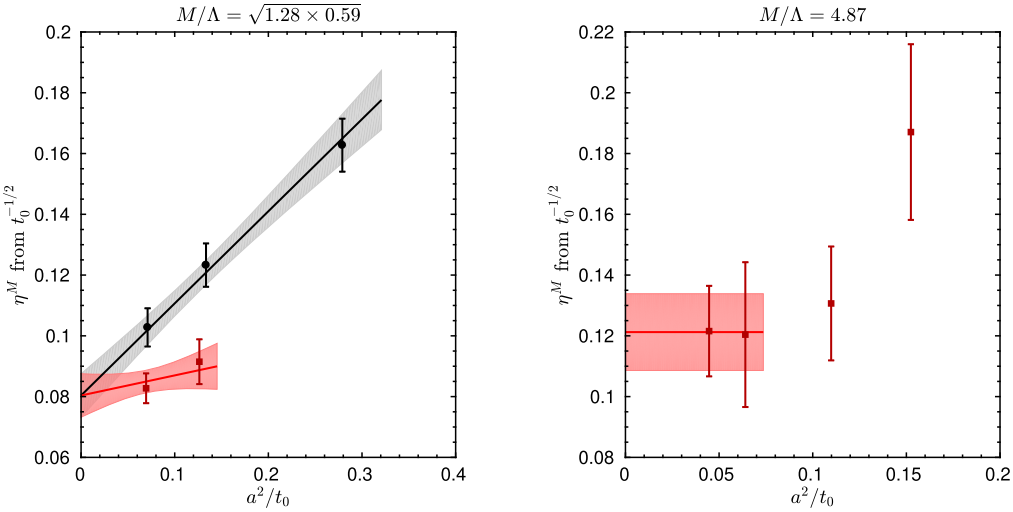

Fig. 11. Examples of continuum limits of $\eta^{\mathrm{M}}(M)$ extracted from $\mathcal{S} = 1/\sqrt{t_0}$ using a linear extrapolation in $a^2/t_0(M)$. In the left plot $\eta^{\mathrm{M}}(\overline{M})$ is computed at $\overline{M}/\Lambda = \sqrt{1.28 \times 0.59}$ using the definition eq. (5.5). Shown are data for standard Wilson (black circles) and twisted mass (red squares) and their combined continuum extrapolation. In the right plot $\eta^{\mathrm{M}}(M)$ is computed at $M = M_{\mathrm{c}}$ ($M/\Lambda = 4.87$) using the definition eq. (5.6).

standard Wilson and twisted mass discretizations. We can also compute a value of $\eta^{\mathrm{M}}(\overline{M})$ at $\overline{M} = \sqrt{4.87 \times 5.7781}$ but its statistical errors are large.

For the case $\mathcal{S} = 1/\sqrt{t_0}$ and $\overline{M} = \sqrt{1.28 \times 0.59}$, the simulation data are shown in the left plot of Fig. 11. The continuum value results from a combined continuum extrapolation linear in $a^2/t_0(M)$. In all our continuum extrapolations we apply the cut $a^2/t_0(M) < 0.32$ to the data to be fitted. The plot shows the continuum extrapolation for both discretizations together with its error bands.

The continuum values of $\eta^{\mathrm{M}}(\overline{M})$ for the various choices of $\mathcal{S}$ are presented in Fig. 12 and plotted against $\Lambda^2/\overline{M}^2$. Notice that the data points corresponding to different quantities $\mathcal{S}$ are slightly displaced horizontally for clarity of presentation. The spread of the data due to $1/M^2$ effects decreases when $\overline{M}$ increases as expected. For comparison we plot in Fig. 12 also the 1-loop (the constant value η_0) and 4-loop (up to the η_3^{M} term) expressions, see eq. (3.23), eq. (3.24) and appendix A.

The mass-scaling function η^{M} can also be computed directly from a simulation at a single quark mass. Using the twisted mass discretization we can rewrite eq. (3.13), for example taking $\mathcal{S} = 1/\sqrt{t_0}$, as

$$-\frac{\mu}{2t_0}\frac{\mathrm{d}t_0}{\mathrm{d}\mu} = \eta^{\mathrm{M}}(M)\,. \tag{5.6}$$

The derivative $\frac{\mathrm{d}t_0}{\mathrm{d}\mu}$ is computed as explained in section 4.2.4. Using $\mathcal{S} = 1/\sqrt{t_c}$ or $1/w_0$ results in determinations of $\eta^{\mathrm{M}}(M)$ similar to eq. (5.6).

In the right plot of Fig. 11 we show the data for the quantity on the left-hand side of eq. (5.6) computed from our simulations at $M = M_{\mathrm{c}}$ ($M/\Lambda = 4.87$) with twisted mass fermions at four values of the lattice coupling $\beta = 6/g_0^2 = 5.6$, 5.7, 5.88 and 6.0. Our fine lattices are needed to control the cut-off effects at this large value of the mass. We perform continuum extrapolations by

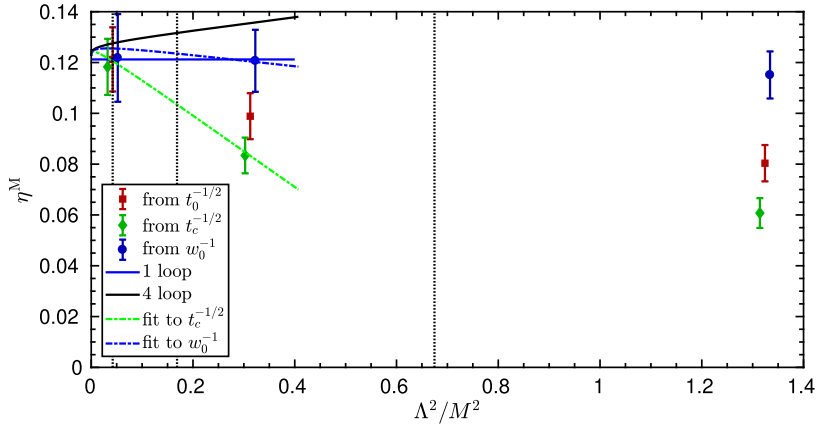

Fig. 12. The mass dependence of the mass-scaling function $\eta^{\rm M}$ in the theory with two mass-degenerate quarks. $\eta^{\rm M}$ is obtained from the hadronic scales $1/\sqrt{t_0}$, $1/\sqrt{t_c}$ and $1/w_0$ and the data for a given mass M are slightly displaced horizontally for clarity. The Monte Carlo data are compared to the perturbative curves. The dash-dotted lines are the fits eq. (6.1) and eq. (6.2) for $1/\sqrt{t_c}$ and $1/w_0$. The vertical dotted lines mark the values of the quark mass $M_{\rm c}$, $M_{\rm c}/2$ and $M_{\rm c}/4$.

"fits" to a constant. Taking three, two or just the last point yields results which are in agreement. We settle for the two-point average which of course has a larger error than the three-point one. The continuum values are plotted in Fig. 12, together with similar determinations of $\eta^{\rm M}(M_{\rm c})$ from $\mathcal{S} = 1/\sqrt{t_c}$ and $1/w_0$. At $M = M_{\rm c}$ the different determinations agree well with each other signaling the smallness of the $1/M^2$ corrections [31].

For our model with two charm quarks we see from Fig. 12 that $\eta^{\rm M}$ is about 1/10, both in perturbation theory and non-perturbatively. For a single charm quark there is an additional factor 1/2. Thus a 2% shift of the charm quark mass leads only to a 1‰ change of a low energy hadronic quantity of mass-dimension one.

The precision of $\eta^{\rm M}(M_{\rm c})$ that we can achieve is around 10%. Within this error the non-perturbative values agree with the perturbative one. This does not look very precise, but in absolute terms this is $\Delta\eta^{\rm M} = 0.01$. We put this into the perspective of phenomenology in the following section.

6. How big are the effects of charm loops?

We recapitulate that the effects of charm loops at low energies come in two classes. One is when we are concerned with dimensionless low energy observables which do not refer to quantities at energies around or above the charm mass. In lattice slang: the quantity is long distance and the lattice spacing a is set through long distance physics in the theory with the heavy quark. In this case the value of the Λ-parameter drops out and the only effects of the heavy quark mass are due to the power corrections originating from $\mathcal{L}_2$ studied in [11,31]. These effects are very small. To be specific, when decoupling two charm quarks, the power corrections in ratios of hadronic scales eq. (4.8) were found to be approximately 0.4%.

The prototype for the second class is given by the connection of the fundamental scales of the four-flavor and the three-flavor theory. In our model it is the connection between the two-flavor theory and the zero-flavor theory. The very relevant question is what the uncertainty is when one uses the perturbatively computed $P_{\ell,{\rm f}}(M/\Lambda_{\rm f})$. In section 3.3 we have seen that 3,4,5-loop

corrections are very small. How big can non-perturbative effects be? The close agreement of our non-perturbative $\eta^{\rm M}$ (section 5.2) with perturbation theory and the dashed curve in Fig. 10 with the non-perturbative points shows that they are small. We now put this into numbers, estimating the non-perturbative effects to $\eta^{\rm M}$ and to $P_{\ell,{\rm f}}(M/\Lambda_{\rm f})$ in our model calculation with $N_{\rm f}=2$, $N_\ell=0$. As will become clear, these estimates are rough and, depending on the assumptions made, can vary quite a bit. Still, their smallness can be quantified at a reasonable level.

6.1. Non-perturbative effects on $\eta^{\rm M}$ and $P_{0,2}$

In Fig. 12 we include dash-dotted curves corresponding to the fits

$$\eta^{\rm M} = \eta^{\rm M}_{\rm pert} + \eta^{{\rm M},\mathcal{S}}_{\rm NP}\,, \tag{6.1}$$

where $\eta^{\rm M}_{\rm pert}$ is the 4-loop expression and $\eta^{{\rm M},\mathcal{S}}_{\rm NP}$ the remainder, which depends on the quantity $\mathcal{S}$. As a first estimate of the non-perturbative contribution we assume that $\eta^{{\rm M},\mathcal{S}}_{\rm NP}$ is dominated by the terms in $\mathcal{L}_2$ and neglect the logarithmic (in M/Λ) corrections. This means we assume

$$\eta^{{\rm M},\mathcal{S}}_{\rm NP} = c^{\mathcal{S}}\,\frac{\Lambda^2}{M^2} \tag{6.2}$$

for large masses. Note that the fit function eq. (6.1) has the correct asymptotics

$$\lim_{M\to\infty}\eta^{\rm M} = \eta_0\,, \tag{6.3}$$

as guaranteed by asymptotic freedom in the form $\lim_{M\to\infty} g_*=0$. In Fig. 12 we compare fits for $\mathcal{S}=1/\sqrt{t_c}$ and $\mathcal{S}=1/w_0$. The fits include the Monte Carlo data of $\eta^{\rm M}$ for $M/\Lambda=4.87$ (the charm-quark mass) and $M/\Lambda=\sqrt{2.50\times1.28}=1.8$. They yield the values $c^{1/\sqrt{t_c}}=-0.167(22)$ and $c^{1/w_0}=-0.048(39)$. In the following we will take $c=-0.2$, which is a conservative choice accommodating both values and their errors. Covering the end of the error bars at the charm would require values of $|c|$ larger by a factor two to three.

We recall from eq. (3.12) that the mass scaling function is defined as $\eta^{\rm M}\equiv\left.\frac{\partial\log(P_{0,2})}{\partial x}\right|_{\Lambda}$, with $x=\log(M/\Lambda)$. The effect of the $\frac{\Lambda^2}{M^2}$ term on $P_{0,2}(M/\Lambda)$,

$$\Delta\log(P_{0,2}) \equiv \log\big[P_{0,2}(M/\Lambda)\big] - \log\Big[\,P_{0,2}(M/\Lambda)\big|_{\rm pert}\Big] \tag{6.4}$$

$$= -\int\limits_{\log(M/\Lambda)}^{\infty} h(x){\rm d}x\,, \quad \text{with } h(\log(M/\Lambda)) = \eta^{\rm M} - \eta^{\rm M}_{\rm pert}\,, \tag{6.5}$$

is easily evaluated. From $h(x)=c\,{\rm e}^{-2x}$ one has

$$\Delta\log(P_{0,2}) = -\frac{c}{2}\,\frac{\Lambda^2}{M^2}\,. \tag{6.6}$$

Note that due to the asymptotics eq. (6.3) the contribution to eq. (6.4) from the integration limit at ∞ cancels in the difference. Inserting $c=-0.2$ and the approximate charm-quark mass value $\frac{\Lambda^2}{M_{\rm c}^2}\approx 1/25$ yields $\Delta\log(P_{0,2})=0.004$. This means a 0.4% change (or better uncertainty) due to non-perturbative effects of the described form and magnitude. In other words a 0.4% precision for perturbation theory in the conversion of the Λ-parameter. We consider this a good estimate, but

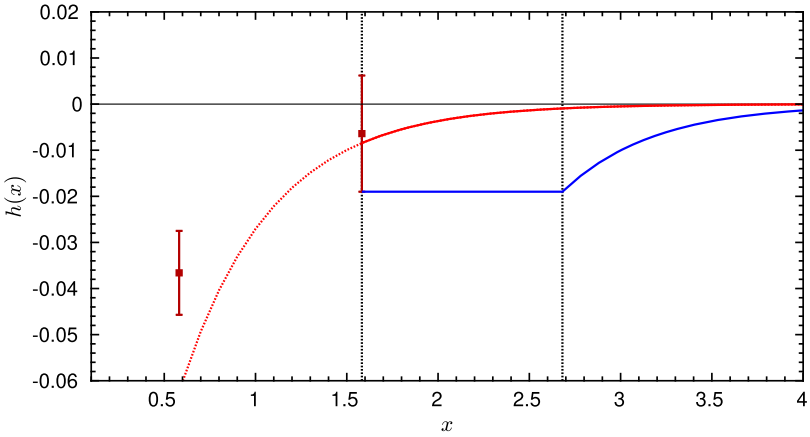

Fig. 13. The integrand of eq. (6.5) for the scale $\mathcal{S} = 1/\sqrt{t_0}$. Data points are $\eta^{\mathrm{M}} - \eta^{\mathrm{M}}_{\mathrm{pert}}$. The red line corresponds to the estimate eq. (6.6) and the blue line represents eq. (6.10) together with the $\exp(-2x)$ decay from $M = 3M_{\mathrm{c}}$ on. The vertical dotted lines mark the values of the quark mass M_{c} and $3M_{\mathrm{c}}$.

it clearly depends on the assumptions made. Therefore, we present a second, very conservative, estimate.

As illustrated in Fig. 13, we split the integral into

$$\Delta \log(P_{0,2}) = A + B\,, \tag{6.7}$$

$$A = -\int_{\log(M/\Lambda)}^{\log(M_{\mathrm{pert}}/\Lambda)} h(x)\mathrm{d}x\,, \tag{6.8}$$

$$B = -\int_{\log(M_{\mathrm{pert}}/\Lambda)}^{\infty} h(x)\mathrm{d}x\,, \tag{6.9}$$

where M_{pert} is high enough such that h and therefore B can be neglected or replaced by the previous estimate. For the lower mass region we just bound

$$|A| \leq \log(M_{\mathrm{pert}}/M)\, h_{\mathrm{max}}\,, \tag{6.10}$$

where h_{max} is the maximum of $|h(x)|$ in the interval $\log(M/\Lambda) \leq x \leq \log(M_{\mathrm{pert}}/\Lambda)$. Numerical information is now obtained by making the reasonable assumption that beyond the masses that we have reached η^{M} continues approaching the perturbative one. We can then replace h_{max} by what we find for our largest mass, $\eta^{\mathrm{M}}(M_{\mathrm{c}}/\Lambda) - \eta^{\mathrm{M}}_{\mathrm{pert}}(M_{\mathrm{c}}/\Lambda) = -0.006(13)$ or $|h| \leq 0.019$. Further setting $M_{\mathrm{pert}} = 3M_{\mathrm{c}}$ where $1/M^2$ terms are suppressed by an order of magnitude compared to at M_{c}, we arrive at $|A| \leq 0.021$. We here took the scale $\mathcal{S} = 1/\sqrt{t_0}$ but the others yield numbers which are very close. Given that no decay of $|h|$ is used this is likely an overestimate of the integral and we neglect the small piece B. We thus cite as the conservative estimate

$$\Delta \log(P_{0,2}) = 0.02\,, \tag{6.11}$$

a 2% non-perturbative contribution to $P_{0,2}$.

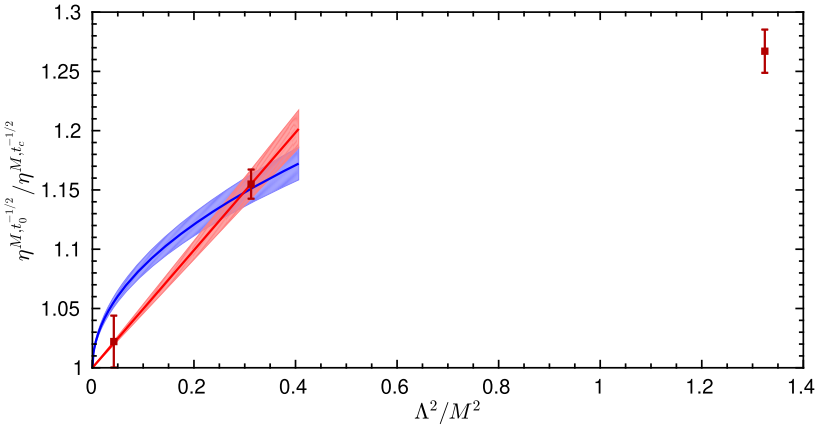

Fig. 14. The ratio eq. (6.12) of the mass-dependence function η^{M} computed from the hadronic scales $\mathcal{S}_1 = 1/\sqrt{t_0}$ and $\mathcal{S}_2 = 1/\sqrt{t_c}$. The lines in the red and blue bands are fits assuming leading non-perturbative effects proportional to $(\Lambda/M)^2$ and Λ/M respectively.

6.2. *Power corrections*

In eq. (6.2) we made the assumption that the non-perturbative effects are dominated by the leading $(\Lambda/M)^2$ ones for our largest masses. It was tested in [31] for ratios of two different hadronic scales $\mathcal{S}_1/\mathcal{S}_2$ in the same mass-range. We corroborate it for the case of η^{M} by computing the ratio

$$R = \frac{\eta^{\mathrm{M},\,\mathcal{S}_1}}{\eta^{\mathrm{M},\,\mathcal{S}_2}} \tag{6.12}$$

of η^{M} calculated as in eq. (3.13) from two different hadronic scales. Using eq. (6.1) and eq. (6.5) we see that $R = 1 + (h^{\mathcal{S}_1} - h^{\mathcal{S}_2})/\eta^{\mathrm{M}}_{\mathrm{pert}} + \mathrm{O}(h^2)$. In Fig. 14 we show the results for the choice $\mathcal{S}_1 = 1/\sqrt{t_0}$ and $\mathcal{S}_2 = 1/\sqrt{t_c}$. The line in the red band is a fit to the two largest mass points using the assumption in eq. (6.2) and neglecting higher order terms in R. It yields $h^{1/\sqrt{t_0}} - h^{1/\sqrt{t_c}} = 0.50(4) \times (\Lambda/M)^2 \cdot \eta^{\mathrm{M}}_{\mathrm{pert}}$ with a χ^2 per degree of freedom equal to 0.003. For comparison we also show the line in the blue band which corresponds to non-perturbative effects proportional to Λ/M. It yields $h^{1/\sqrt{t_0}} - h^{1/\sqrt{t_c}} = 0.27(2) \times \Lambda/M \cdot \eta^{\mathrm{M}}_{\mathrm{pert}}$ with a worse χ^2 per degree of freedom equal to 2.4.

We can use the fits to the ratio R to estimate the size of non-perturbative effects in the difference of $\log(P_{0,2})$ extracted from $\mathcal{S}_1$ and $\mathcal{S}_2$:

$$\log\left[P^{\mathcal{S}_1}_{0,2}(M/\Lambda)\right] - \log\left[P^{\mathcal{S}_2}_{0,2}(M/\Lambda)\right] = -\int_{\log(M/\Lambda)}^{\infty} \left[h^{\mathcal{S}_1}(x) - h^{\mathcal{S}_2}(x)\right] \mathrm{d}x\,. \tag{6.13}$$

Evaluating the integral with a constant $\eta^{\mathrm{M}}_{\mathrm{pert}} \approx \eta^{\mathrm{M}}_{\mathrm{pert}}(M_{\mathrm{c}}) = 0.1276$ and $\frac{\Lambda}{M_{\mathrm{c}}} \approx 1/5$ yields the values -0.0013 (fit $h^{1/\sqrt{t_0}} - h^{1/\sqrt{t_c}} \sim (\Lambda/M)^2$) and -0.0069 (fit $h^{1/\sqrt{t_0}} - h^{1/\sqrt{t_c}} \sim \Lambda/M$) for the difference of $\log(P_{0,2})$ eq. (6.13). This difference is a further test of the non-perturbative effects. The absolute values are significantly smaller than the conservative estimate in eq. (6.11), confirming the latter.

6.3. Heavy quark content of the nucleon

The matrix element of the scalar heavy quark density between nucleon states is a relevant contribution to the cross-section for the scalar interaction of dark matter with ordinary matter [59]. It can be related, by the Hellmann–Feynman theorem, to the derivative of the nucleon mass m_N with respect to the heavy quark mass. In the chiral limit for the up, down and strange quark and up to $O(\Lambda^2/M_q^2)$ this derivative is the mass-scaling function η^{M}, see eq. (3.13),

$$\frac{1}{m_N}\langle N|m_{q,0}(\bar{q}q)_0|N\rangle = \frac{1}{m_N}\langle N|M_q(\bar{q}q)_{\mathrm{RGI}}|N\rangle = \eta^{\mathrm{M}} + O(\Lambda^2/M_q^2)\,, \tag{6.14}$$

where $m_{q,0}$ is the bare heavy quark mass and $(\bar{q}q)_0$ is the bare scalar density of quark q, and $(\bar{q}q)_{\mathrm{RGI}}$ is the RGI-renormalized scalar heavy quark density. Our result in Fig. 12 shows that perturbation theory can be safely applied to compute η^{M} as it was done in [15,60,61] and non-perturbative effects in η^{M} are below $0.02/2$ for the case of a single charm quark as just discussed.

6.4. From the model to QCD

Note that currently the precision for the Λ-parameter is at the level of around 4% [18,62]. This sets the scale for what is small and what is big. Furthermore, there is no reason why our toy-model computation should give a significantly different result for the magnitude (not the details) of non-perturbative effects except that we have decoupled *two* heavy quarks. Indeed, since we are dealing with small effects of quark loops, it is very plausible that the effect of more than one quark-loop effects are smaller than the ones of a single quark loop, which scales proportionally to the number of quarks. We are here just counting quark loops in arbitrary gauge backgrounds, so the argument is valid independently of whether the gauge coupling is large or small. It is non-perturbative. It means that these small effects will be about a factor two smaller for the decoupling of the charm-quark in QCD, compared to the studied model. We use this for the magnitude of all effects, also for the uncertainty of perturbation theory.

We saw in Table 1 that the dependence on the number of light quarks of η^{M} between $N_\ell = 0$ and $N_\ell = 3$ amounts to about 20% at leading order in perturbation theory. For this reason we include a safety margin of 50% in our estimate of non-perturbative effects $h_{\max}$, see eq. (6.10). We conclude that one can *safely* neglect non-perturbative effects all-together for connecting three-flavor and four-flavor Λ at a level down to

$$\Delta\log(P_{3,4}) = 0.015\,, \tag{6.15}$$

a 1.5% non-perturbative contribution to $P_{3,4}$.

In the same way non-perturbative effects to eq. (6.14) are estimated to be below $1.5 \times h_{\max}/2 = 0.014$ in QCD when q is the charm quark.

7. Conclusions

In this article we presented a numerical study of the decoupling of heavy quarks. In particular we study the dependence of hadronic, low energy quantities on the mass M of the decoupled heavy quark. We define and compute in perturbation theory a mass-dependence function η^{M} eq. (3.13). This computation is performed in leading order in the effective theory which describes the decoupling of the heavy quarks at low energy. We study the behavior of perturbation theory for the function η^{M} and show that perturbation theory by itself suggests that it is well within the

region of asymptotic convergence even for the case of decoupling a charm quark. We remark that $\eta^{\rm M}$ can be related to the heavy quark content of the nucleon, see eq. (6.14), which is a relevant input for dark matter searches.

To test the applicability of perturbation theory at the charm quark mass we compare the mass dependence of the ratio $\sqrt{t_0(M)/t_0(0)}$ defined in terms of the hadronic scale $1/\sqrt{t_0}$ to the perturbative prediction, see Fig. 10. We also determine the mass-scaling function $\eta^{\rm M}$ non-perturbatively, see Fig. 12. In order to be able to control the continuum extrapolations and have precise results we do this in a model consisting of two mass-degenerate quarks whose mass ranges up to the charm quark mass. The non-perturbative mass dependence agrees with the perturbative prediction at a level of about 10% for the small mass-scaling function $\eta^{\rm M}$ computed at the charm quark mass. This means that we confirm that a 2% shift of the charm quark mass leads only to a 1‰ change of a low energy hadronic quantity of mass-dimension one. We explained in section 6 that this precision is good enough to conclude that at the charm mass, the function $P_{\ell,\rm f}$ in eq. (3.9) can be predicted by perturbation theory with 2% accuracy for $N_{\rm f}=2,\ N_\ell=0$ and 1.5% accuracy for $N_{\rm f}=4,\ N_\ell=3$. This allows to predict

$$\frac{\Lambda_{\overline{\rm MS}}\sqrt{t_0(0)}\big|_{N_{\rm f}=2}}{\Lambda_{\overline{\rm MS}}\sqrt{t_0}\big|_{N_\ell=0}} = 1.134(28)\,. \tag{7.1}$$

Moreover we estimate that the non-perturbative effects in $\eta^{\rm M}$ are below 0.014 for the charm quark. These numbers are for the blue curve in Fig. 13, while we think that the red curve $\sim 1/M^2$ is more realistic; it yields non-perturbative uncertainties which are a factor five smaller for $P_{\ell,\rm f}$.

On the other hand, in the direct comparison of $\sqrt{t_0(M_c)/t_0(0)}$ to the product $Q\,P$, eq. (3.10) we presently have only 10% accuracy because in the literature the ratio, Q is not known more precisely.

Our most important conclusion concerns phenomenology: the ratio of three-flavor and four-flavor Λ-parameters can be computed in perturbation theory with a precision of 1.5% or better. Power corrections $\sim 1/M_{\rm c}^2$ were found to be much smaller in low energy observables [11,31]. This means that the Λ-parameter of the five-flavor theory is safely predicted at the 1-2 percent level from three-flavor low energy physics once the running of the coupling is under control [63], see section 6.4 for details. Note that the present precision of $\Delta\alpha_{\overline{\rm MS}}(M_{\rm Z})=0.0008$ of [63] corresponds to 3.5% in the Λ-parameter. Thus, there is plenty of room for relevant improvement within the three-flavor theory.

Similarly we conclude that non-perturbative effects to the charm quark content of the nucleon, eq. (6.14) are below 0.014.

Acknowledgements

We thank M. Bruno and J. Heitger for their inputs for our analyses. We thank M. Dalla Brida and A. Ramos for providing valuable feedback on the manuscript. We gratefully acknowledge the computer resources granted by the John von Neumann Institute for Computing (NIC) and provided on the supercomputer JUROPA at Jülich Supercomputing Centre (JSC) and by the Gauss Centre for Supercomputing (GCS) through the NIC on the GCS share of the supercomputer JUQUEEN at JSC, with funding by the German Federal Ministry of Education and Research (BMBF) and the German State Ministries for Research of Baden-Württemberg (MWK), Bayern (StMWFK) and Nordrhein-Westfalen (MIWF). We are further grateful for computer time allocated for our project on the Konrad and Gottfried computers at the North-German Supercomputing Alliance HLRN, on the CHEOPS, a scientific supercomputer sponsored by the DFG

of the regional computing centre of the University of Cologne (RRZK), the Stromboli cluster at the University of Wuppertal and the PAX cluster at DESY, Zeuthen. This work is supported by the Deutsche Forschungsgemeinschaft in the SFB/TR 55 and is based on previous work [11] supported also by the SFB/TR 09. FK thanks CERN for hospitality.

Appendix A. Expansion of the matching condition and the mass scaling function

The coefficients of the matching of the coupling (3.15) can be found in [4,16,64]. We collect here all known coefficients for convenience. Note that we use the particular scale $\mu = m_*$, for which logarithms $\log(\mu/\overline{m}(\mu))$ vanish and $c_1 = 0$. The two loop coefficient is known for arbitrary N_f, N_ℓ

$$c_2 = (N_\mathrm{f} - N_\ell)\,\frac{11}{72}\,(4\pi^2)^{-2}\,. \tag{A.1}$$

The three loop one is known for $N_\mathrm{f} - N_\ell = 1, 2$

$$c_3 = \left[1.881732 - 0.169303\,N_\ell\right](4\pi^2)^{-3} \quad \text{for } N_\mathrm{f} - N_\ell = 2\,, \tag{A.2}$$

$$c_3 = \left[0.972057 - 0.084651\,N_\ell\right](4\pi^2)^{-3} \quad \text{for } N_\mathrm{f} - N_\ell = 1\,, \tag{A.3}$$

and the four loop one only for $N_\mathrm{f} - N_\ell = 1$

$$c_4 = \left[5.170347 - 1.009932 N_\ell - 0.021978\,{N_\ell}^2\right](4\pi^2)^{-4} \quad \text{for } N_\mathrm{f} - N_\ell = 1\,. \tag{A.4}$$

The coefficients of the expansion of the mass scaling function (3.21) are obtained by expanding (3.19). Up to four loop they are given by

$$\eta_0 = 1 - \frac{b_0(N_\mathrm{f})}{b_0(N_\ell)}\,, \tag{A.5}$$

$$\eta_1 = (\eta_0 - 1)\left[\tilde{b}_1(N_\mathrm{f}) - \tilde{b}_1(N_\ell)\right], \tag{A.6}$$

$$\eta_2 = (\eta_0 - 1)\left[c_2 + \tilde{b}_2(N_\mathrm{f}) - \tilde{b}_2(N_\ell)\right] - \tilde{b}_1(N_\ell)\eta_1 \tag{A.7}$$

$$\eta_3 = (\eta_0 - 1)\left[2c_3 + \tilde{b}_3(N_\mathrm{f}) - \tilde{b}_3(N_\ell)\right] - \tilde{b}_1(N_\ell)\eta_2 + \left(c_2 - \tilde{b}_2(N_\ell)\right)\eta_1 \tag{A.8}$$

$$\begin{aligned}\eta_4 = {} & (\eta_0 - 1)\left[3c_4 + \tilde{b}_4(N_\mathrm{f}) - \tilde{b}_4(N_\ell) + \tilde{b}_1(N_\mathrm{f})c_3 - c_2\left(4c_2 + \tilde{b}_2(N_\ell)\right)\right] \\ & -\tilde{b}_1(N_\ell)\eta_3 + \left(c_2 - \tilde{b}_2(N_\ell)\right)\eta_2 + \left(c_3 - \tilde{b}_3(N_\ell)\right)\eta_1\,.\end{aligned} \tag{A.9}$$

The evaluation of the coefficients requires the knowledge of the β-function of the coupling up to five loops [6–10].

The coefficients of the function (3.23) are straightforwardly obtained from (3.24). Their evaluation requires in addition the anomalous dimension up to four loops [65,66].

Appendix B. Asymptotic expression for $P(M/\Lambda)$

In this section we derive the asymptotic expression eq. (3.26). Starting point is the definition of $P(M/\Lambda)$ as the ratio of the Λ-parameters. We are interested in the asymptotic behavior at large M/Λ. Since our matching/renormalization scale $\mu = m_*$ is tied to the mass $\overline{m}(m_*) = m_*$, large M/Λ means small $g_* = \bar{g}(m_*)$, cf. section 3.2. Therefore we neglect terms $\mathrm{O}(g_*^2)$. Using eq. (3.1) one obtains (see also eq. (3.28))

Table 4
Overview of the ensembles generated with $N_f = 2$ O(a) improved Wilson fermions. The columns show the lattice sizes, the gauge coupling $\beta = 6/g_0^2$, the boundary conditions (periodic (p) or open (o)), the hopping parameter κ (which is related to the bare mass m_0 through $\kappa = 1/(2am_0 + 8)$), the PCAC mass am, the ratio of the RGI mass M to the Λ parameter (computed using eq. (4.10)), the scales r_0/a and t_0/a^2 and the total statistics in molecular dynamics units.

$\frac{T}{a} \times \left(\frac{L}{a}\right)^3$	β	BC	κ	am	M/Λ	r_0/a	t_0/a^2	kMDU
64×32^3	5.3	p	0.13550	0.03405(8)	0.638(46)	5.903(36)	3.481(14)	1
64×32^3	5.3	p	0.13450	0.06979(7)	1.308(95)	5.193(20)	2.714(14)	2
64×32^3	5.3	p	0.13270	0.13873(8)	2.600(189)	4.270(6)	1.842(3)	2
120×32^3	5.5	o	0.136020	0.02467(4)	0.630(46)	8.49(12)	7.318(36)	8
120×32^3	5.5	o	0.135236	0.05022(3)	1.282(93)	7.580(44)	6.092(21)	8
96×48^3	5.5	p	0.133830	0.09614(2)	2.454(178)	6.787(19)	4.867(12)	4
192×48^3	5.7	o	0.136200	0.01691(2)	0.586(43)	11.48(24)	14.02(6)	4
192×48^3	5.7	o	0.135570	0.03683(2)	1.277(94)	10.53(12)	11.87(7)	4
192×48^3	5.7	o	0.134450	0.07209(2)	2.500(184)	9.50(5)	9.821(36)	8

$$\log[P(M/\Lambda)] = \log(\Lambda_\ell/m_*) - \log(\Lambda_f/m_*) \tag{B.1}$$
$$= I_g^\ell(g_* \widetilde{C}(g_*)) - I_g^f(g_*)\,, \tag{B.2}$$
$$= \frac{\eta_0}{2b_0(N_f)g_*^2} - \frac{b_1(N_\ell)}{2b_0(N_\ell)^2}\log(b_0(N_\ell)g_*^2) \tag{B.3}$$
$$+ \frac{b_1(N_f)}{2b_0(N_f)^2}\log(b_0(N_f)g_*^2) + \mathrm{O}(g_*^2)\,. \tag{B.4}$$

In order to replace the coupling we extract the asymptotic relation between g_* and M/Λ from eq. (3.31). Using the shorthands $L_M = \log(M/\Lambda)$ and $x = 2b_0(N_f)g_*^2$ the relation up to $\mathrm{O}(g_*^2)$ is

$$L_M = \frac{1}{x} - \frac{d_0}{2b_0(N_f)}\log(x) + \frac{b_1(N_f)}{2b_0(N_f)^2}\log(x/2) + \mathrm{O}(x)\,. \tag{B.5}$$

Taking the logarithm on both sides yields $\log(L_M) = -\log(x) + \mathrm{O}(x\log(x))$. Inverting gives the result

$$\frac{1}{x} = L_M + \frac{d_0}{2b_0(N_f)}\log(L_M) - \frac{b_1(N_f)}{2b_0(N_f)^2}\log(L_M/2) + \mathrm{O}\left(\frac{\log(L_M)}{L_M}\right)\,. \tag{B.6}$$

Using these relations g_* can be eliminated from (B.3)-(B.4) and one arrives at eq. (3.26).

Appendix C. Simulation parameters

Table 4 and Table 5 summarize the parameters of our simulations of $N_f = 2$ mass-degenerate quarks using O(a) improved standard Wilson fermions and twisted mass Wilson fermions at maximal twist respectively.

In Table 6 we list the values of the hadronic scale L_1/a [19,32]. At $\beta = 5.3,\ 5.5$ they are taken from Table 7 of [19]. At the other β values they are obtained from a quadratic fit in β of $\ln(L_1/a)$, where data for the latter are taken from Table 13 of [19]. The lattice spacing for $\beta > 5.5$ (not covered by the simulations in [19]) can be inferred from the value $L_1 = 0.400(10)$fm determined in [19].

Table 5
Overview of the ensembles generated with $N_f = 2$ twisted mass fermions at maximal twist. The columns show the lattice sizes, the gauge coupling $\beta = 6/g_0^2$, the hopping parameter κ (for maximal twist), the twisted mass parameter $a\mu$, the ratio of the RGI mass M to the Λ parameter (computed using eq. (4.10)), the scales r_0/a (where it is measured) and t_0/a^2 and the total statistics in molecular dynamics units.

$\frac{T}{a} \times \left(\frac{L}{a}\right)^3$	β	κ	$a\mu$	M/Λ	r_0/a	t_0/a^2	kMDU
120×32^3	5.300	0.136457	0.024505	0.5900	–	4.174(13)	4.3
120×32^3	5.500	0.1367749	0.018334	0.5900	8.77(15)	7.917(82)	8
192×48^3	5.700	0.136687	0.013713	0.5900	–	14.40(10)	5.8
120×32^3	5.500	0.1367749	0.039776	1.2800	8.010(62)	6.871(33)	8
192×48^3	5.700	0.136687	0.029751	1.2800	–	12.668(39)	16.2
120×32^3	5.500	0.1367749	0.077687	2.5000	7.392(62)	5.836(27)	8
192×48^3	5.700	0.136687	0.058108	2.5000	–	10.916(38)	9
192×48^3	5.600	0.136710	0.130949	4.8700	–	6.561(12)	16
120×32^3	5.700	0.136698	0.113200	4.8703	9.123(57)	9.104(36)	17.2
192×48^3	5.880	0.136509	0.087626	4.8700	11.946(55)	15.622(62)	23.1
192×48^3	6.000	0.136335	0.072557	4.8700	14.34(10)	22.39(12)	22.4
192×48^3	5.600	0.136710	0.155367	5.7781	–	6.181(11)	2.1
192×48^3	5.700	0.136687	0.1343	5.7781	–	8.565(31)	2.7
120×32^3	5.880	0.136509	0.103965	5.7781	–	14.916(93)	59.9

Table 6
The values of the scale L_1/a used in our simulations and the corresponding lattice spacings.

β	L_1/a	a [fm]
5.30	6.195(51)	0.066
5.50	8.280(80)	0.049
5.60	9.569(99)	≈0.042
5.70	11.07(17)	≈0.036
5.88	14.30(24)	≈0.028
6.00	17.27(70)	≈0.023

C.1. Mass corrections

The data for a hadronic scale $\mathcal{S}$ such as $r_0^{-1}, t_0^{-1/2}$ obtained from the simulations with standard Wilson fermions are corrected for small mismatches of the values M/Λ compared to the target values M_t/Λ given in eq. (4.1), see Table 4. This is done by fitting the $\beta = 5.7$ data to the form

$$a\mathcal{S}(M) = s_1 \times (M/\Lambda)^{\alpha} , \tag{C.1}$$

with fit coefficients s_1 and α. This fit formula is motivated by eq. (3.10) taking the asymptotic expression $P = (M/\Lambda_f)^{\eta_0}$. For example for $\mathcal{S} = 1/\sqrt{t_0}$ we get $\alpha = 0.123(2)$ and for $\mathcal{S} = 1/r_0$ we get $\alpha = 0.139(12)$ which are close to $\eta_0 = 0.121212$. The corrected values $\mathcal{S}(M_t)$ are computed as

$$\ln(a\mathcal{S}(M_t)) = \ln(a\mathcal{S}(M)) + \alpha \ln(M_t/M) . \tag{C.2}$$

Note that eq. (C.2) being a small correction is applied for all lattice spacings a. Moreover the Λ parameter drops out in eq. (C.2). Since the main contribution to the error on M/Λ comes from ΛL_1, it does not affect the mass corrections. In order to determine the final error of $a\mathcal{S}(M_t)$, we propagate the error of the exponent α and linearly add its contribution (for a conservative estimate) multiplied by a factor of two.

No corrections are needed for the hadronic scales from twisted mass simulations since their parameters are tuned for the target mass values, see section 4.2.3.

References

[1] M. Lüscher, Properties and uses of the Wilson flow in lattice QCD, J. High Energy Phys. 08 (2010) 071, arXiv:1006.4518.
[2] S. Weinberg, Effective gauge theories, Phys. Lett. B 91 (1980) 51.
[3] W. Bernreuther, W. Wetzel, Decoupling of heavy quarks in the minimal subtraction scheme, Nucl. Phys. B 197 (1982) 228.
[4] K. Chetyrkin, J.H. Kühn, C. Sturm, QCD decoupling at four loops, Nucl. Phys. B 744 (2006) 121, arXiv:hep-ph/0512060.
[5] Y. Schröder, M. Steinhauser, Four-loop decoupling relations for the strong coupling, J. High Energy Phys. 01 (2006) 051, arXiv:hep-ph/0512058.
[6] T. van Ritbergen, J.A.M. Vermaseren, S.A. Larin, The Four loop beta function in quantum chromodynamics, Phys. Lett. B 400 (1997) 379, arXiv:hep-ph/9701390.
[7] M. Czakon, The four-loop QCD beta-function and anomalous dimensions, Nucl. Phys. B 710 (2005) 485, arXiv:hep-ph/0411261.
[8] P.A. Baikov, K.G. Chetyrkin, J.H. Kühn, Five-loop running of the QCD coupling constant, Phys. Rev. Lett. 118 (2017) 082002, arXiv:1606.08659.
[9] T. Luthe, A. Maier, P. Marquard, Y. Schröder, Towards the five-loop Beta function for a general gauge group, J. High Energy Phys. 07 (2016) 127, arXiv:1606.08662.
[10] F. Herzog, B. Ruijl, T. Ueda, J.A.M. Vermaseren, A. Vogt, The five-loop beta function of Yang-Mills theory with fermions, J. High Energy Phys. 02 (2017) 090, arXiv:1701.01404.
[11] ALPHA collaboration, M. Bruno, J. Finkenrath, F. Knechtli, B. Leder, R. Sommer, Effects of heavy sea quarks at low energies, Phys. Rev. Lett. 114 (2015) 102001, arXiv:1410.8374.
[12] S. Sint, Lattice QCD with a chiral twist, in: Perspectives in Lattice QCD, World Scientific, 2007, pp. 169–208, arXiv:hep-lat/0702008.
[13] R. Sommer, A new way to set the energy scale in lattice gauge theories and its applications to the static force and α_s in SU(2) Yang-Mills theory, Nucl. Phys. B 411 (1994) 839, arXiv:hep-lat/9310022.
[14] S. Borsanyi, S. Dürr, Z. Fodor, C. Hoelbling, S.D. Katz, et al., High-precision scale setting in lattice QCD, J. High Energy Phys. 1209 (2012) 010, arXiv:1203.4469.
[15] A. Kryjevski, Heavy quark anti-q q matrix elements in the nucleon from perturbative QCD, Phys. Rev. D 70 (2004) 094028, arXiv:hep-ph/0312196.
[16] A.G. Grozin, M. Hoeschele, J. Hoff, M. Steinhauser, Simultaneous decoupling of bottom and charm quarks, J. High Energy Phys. 1109 (2011) 066, arXiv:1107.5970.
[17] R. Sommer, Introduction to non-perturbative heavy quark effective theory, in: Modern Perspectives in Lattice QCD: Quantum Field Theory and High Performance Computing. Proceedings, International School, 93rd Session, Les Houches, France, August 3-28, 2009, 2010, pp. 517–590, arXiv:1008.0710.
[18] Particle Data Group collaboration, C. Patrignani, et al., Review of particle physics, Chin. Phys. C 40 (2016) 100001.
[19] P. Fritzsch, F. Knechtli, B. Leder, M. Marinkovic, S. Schaefer, et al., The strange quark mass and Lambda parameter of two flavor QCD, Nucl. Phys. B 865 (2012) 397, arXiv:1205.5380.
[20] J. Heitger, G.M. von Hippel, S. Schaefer, F. Virotta, Charm quark mass and D-meson decay constants from two-flavour lattice QCD, PoS LATTICE2013 (2014) 475, arXiv:1312.7693.
[21] C.W. Bernard, T. Burch, K. Orginos, D. Toussaint, T.A. DeGrand, et al., The static quark potential in three flavor QCD, Phys. Rev. D 62 (2000) 034503, arXiv:hep-lat/0002028.
[22] R. Narayanan, H. Neuberger, Infinite N phase transitions in continuum Wilson loop operators, J. High Energy Phys. 03 (2006) 064, arXiv:hep-th/0601210.
[23] M. Lüscher, P. Weisz, Perturbative analysis of the gradient flow in non-abelian gauge theories, J. High Energy Phys. 1102 (2011) 051, arXiv:1101.0963.

[24] K.G. Wilson, Confinement of quarks, Phys. Rev. D 10 (1974) 2445.
[25] B. Sheikholeslami, R. Wohlert, Improved continuum limit lattice action for QCD with Wilson fermions, Nucl. Phys. B 259 (1985) 572.
[26] M. Lüscher, S. Sint, R. Sommer, P. Weisz, Chiral symmetry and O(a) improvement in lattice QCD, Nucl. Phys. B 478 (1996) 365, arXiv:hep-lat/9605038.
[27] Alpha collaboration, R. Frezzotti, P.A. Grassi, S. Sint, P. Weisz, Lattice QCD with a chirally twisted mass term, J. High Energy Phys. 08 (2001) 058, arXiv:hep-lat/0101001.
[28] ALPHA collaboration, K. Jansen, R. Sommer, O(a) improvement of lattice QCD with two flavors of Wilson quarks, Nucl. Phys. B 530 (1998) 185, arXiv:hep-lat/9803017.
[29] R. Frezzotti, G.C. Rossi, Chirally improving Wilson fermions. 1. O(a) improvement, J. High Energy Phys. 08 (2004) 007, arXiv:hep-lat/0306014.
[30] P. Dimopoulos, H. Simma, A. Vladikas, Quenched B(K)-parameter from Osterwalder-Seiler tmQCD quarks and mass-splitting discretization effects, J. High Energy Phys. 07 (2009) 007, arXiv:0902.1074.
[31] ALPHA collaboration, F. Knechtli, T. Korzec, B. Leder, G. Moir, Power corrections from decoupling of the charm quark, Phys. Lett. B 774 (2017) 649, arXiv:1706.04982.
[32] ALPHA collaboration, B. Blossier, M. Della Morte, P. Fritzsch, N. Garron, J. Heitger, H. Simma, et al., Parameters of heavy quark effective theory from Nf=2 lattice QCD, J. High Energy Phys. 09 (2012) 132, arXiv:1203.6516.
[33] S. Sint, R. Sommer, The running coupling from the QCD Schrödinger functional: a one loop analysis, Nucl. Phys. B 465 (1996) 71, arXiv:hep-lat/9508012.
[34] M. Lüscher, S. Sint, R. Sommer, P. Weisz, Chiral symmetry and O(a) improvement in lattice QCD, Nucl. Phys. B 478 (1996) 365, arXiv:hep-lat/9605038.
[35] M. Della Morte, R. Sommer, S. Takeda, On cutoff effects in lattice QCD from short to long distances, Phys. Lett. B 672 (2009) 407, arXiv:0807.1120.
[36] M. Dalla Brida, T. Korzec, S. Sint, P. Vilaseca, High precision renormalization of the flavour non-singlet Noether currents in lattice QCD with Wilson quarks, arXiv:1808.09236.
[37] ALPHA collaboration, M. Della Morte, et al., Non-perturbative quark mass renormalization in two-flavor QCD, Nucl. Phys. B 729 (2005) 117, arXiv:hep-lat/0507035.
[38] ALPHA collaboration, M. Della Morte, et al., Computation of the strong coupling in QCD with two dynamical flavours, Nucl. Phys. B 713 (2005) 378, arXiv:hep-lat/0411025.
[39] M. Della Morte, A. Shindler, R. Sommer, On lattice actions for static quarks, J. High Energy Phys. 08 (2005) 051, arXiv:hep-lat/0506008.
[40] M. Donnellan, F. Knechtli, B. Leder, R. Sommer, Determination of the static potential with dynamical fermions, Nucl. Phys. B 849 (2011) 45, arXiv:1012.3037.
[41] A. Hasenfratz, F. Knechtli, Flavor symmetry and the static potential with hypercubic blocking, Phys. Rev. D 64 (2001) 034504, arXiv:hep-lat/0103029.
[42] ETM collaboration, K. Jansen, C. Michael, C. Urbach, The eta-prime meson from lattice QCD, Eur. Phys. J. C 58 (2008) 261, arXiv:0804.3871.
[43] S. Bernardson, P. McCarty, C. Thron, Monte Carlo methods for estimating linear combinations of inverse matrix entries in lattice QCD, Comput. Phys. Commun. 78 (1993) 256.
[44] M. Marinkovic, S. Schaefer, Comparison of the mass preconditioned HMC and the DD-HMC algorithm for two-flavour QCD, PoS LATTICE2010 (2010) 031, arXiv:1011.0911.
[45] ALPHA collaboration, S. Schaefer, R. Sommer, F. Virotta, Critical slowing down and error analysis in lattice QCD simulations, Nucl. Phys. B 845 (2011) 93, arXiv:1009.5228.
[46] ALPHA collaboration, M. Bruno, S. Schaefer, R. Sommer, Topological susceptibility and the sampling of field space in $N_f = 2$ lattice QCD simulations, J. High Energy Phys. 1408 (2014) 150, arXiv:1406.5363.
[47] M. Lüscher, S. Schaefer, Lattice QCD with open boundary conditions and twisted-mass reweighting, Comput. Phys. Commun. 184 (2013) 519, arXiv:1206.2809.
[48] M. Hasenbusch, Speeding up the hybrid Monte Carlo algorithm for dynamical fermions, Phys. Lett. B 519 (2001) 177, arXiv:hep-lat/0107019.
[49] M. Lüscher, Solution of the Dirac equation in lattice QCD using a domain decomposition method, Comput. Phys. Commun. 156 (2004) 209, arXiv:hep-lat/0310048.
[50] A. Frommer, K. Kahl, S. Krieg, B. Leder, M. Rottmann, Adaptive aggregation based domain decomposition multigrid for the lattice Wilson Dirac operator, SIAM J. Sci. Comput. 36 (2014) A1581, arXiv:1303.1377.
[51] C. Alexandrou, S. Bacchio, J. Finkenrath, A. Frommer, K. Kahl, M. Rottmann, Adaptive aggregation-based domain decomposition multigrid for twisted mass fermions, Phys. Rev. D 94 (2016) 114509, arXiv:1610.02370.
[52] H. Panagopoulos, Y. Proestos, The critical hopping parameter in O(a) improved lattice QCD, Phys. Rev. D 65 (2002) 014511, arXiv:hep-lat/0108021.

[53] ALPHA collaboration, U. Wolff, Monte Carlo errors with less errors, Comput. Phys. Commun. 156 (2004) 143, arXiv:hep-lat/0306017.
[54] ALPHA collaboration, F. Knechtli, M. Bruno, J. Finkenrath, B. Leder, R. Sommer, Perturbative versus non-perturbative decoupling of heavy quarks, PoS LATTICE2015 (2016) 256, arXiv:1511.04914.
[55] M. Bruno, R. Sommer, On the N_f-dependence of gluonic observables, PoS LATTICE2013, 321, arXiv:1311.5585.
[56] ALPHA collaboration, S. Capitani, M. Lüscher, R. Sommer, H. Wittig, Non-perturbative quark mass renormalization in quenched lattice QCD, Nucl. Phys. B 544 (1999) 669, arXiv:hep-lat/9810063.
[57] R. Sommer, Scale setting in lattice QCD, PoS LATTICE2013 (2014) 015, arXiv:1401.3270.
[58] O. Bär, M. Golterman, Chiral perturbation theory for gradient flow observables, Phys. Rev. D 89 (2014) 034505, arXiv:1312.4999.
[59] J. Hisano, Effective theory approach to direct detection of dark matter, arXiv:1712.02947.
[60] L. Vecchi, WIMPs and Un-Naturalness, arXiv:1312.5695.
[61] J. Ellis, N. Nagata, K.A. Olive, Uncertainties in WIMP dark matter scattering revisited, Eur. Phys. J. C 78 (2018) 569, arXiv:1805.09795.
[62] S. Aoki, et al., Review of lattice results concerning low-energy particle physics, Eur. Phys. J. C 77 (2017) 112, arXiv:1607.00299.
[63] ALPHA collaboration, M. Bruno, M. Dalla Brida, P. Fritzsch, T. Korzec, A. Ramos, S. Schaefer, et al., QCD coupling from a nonperturbative determination of the three-flavor Λ parameter, Phys. Rev. Lett. 119 (2017) 102001, arXiv:1706.03821.
[64] B.A. Kniehl, A.V. Kotikov, A.I. Onishchenko, O.L. Veretin, Strong-coupling constant with flavor thresholds at five loops in the anti-MS scheme, Phys. Rev. Lett. 97 (2006) 042001, arXiv:hep-ph/0607202.
[65] K.G. Chetyrkin, Quark mass anomalous dimension to $O(\alpha_s^4)$, Phys. Lett. B 404 (1997) 161, arXiv:hep-ph/9703278.
[66] J.A.M. Vermaseren, S.A. Larin, T. van Ritbergen, The four loop quark mass anomalous dimension and the invariant quark mass, Phys. Lett. B 405 (1997) 327, arXiv:hep-ph/9703284.